Biochem. J. (2014) **459**, 525–538 (Printed in Great Britain) doi:10.1042/BJ20140017

Structural and mechanistic insights into an extracytoplasmic copper trafficking pathway in *Streptomyces lividans*

Katie L. I. M. BLUNDELL*, Michael A. HOUGH*, Erik VIJGENBOOM† and Jonathan A. R. WORRALL*[1]

*School of Biological Sciences, University of Essex, Wivenhoe Park, Colchester CO4 3SQ, U.K.
†Molecular Biotechnology, Institute of Biology, Sylvius Laboratory, Leiden University, PO Box 9505, 2300RA Leiden, The Netherlands

In *Streptomyces lividans* an extracytoplasmic copper-binding Sco protein plays a role in two unlinked processes: (i) initiating a morphological development switch and (ii) facilitating the co-factoring of the Cu_A domain of CcO (cytochrome *c* oxidase). How Sco obtains copper once secreted to the extracytoplasmic environment is unknown. In the present paper we report on a protein possessing an $HX_6MX_{21}HXM$ motif that binds a single cuprous ion with subfemtomolar affinity. High-resolution X-ray structures of this extracytoplasmic copper chaperone-like protein (ECuC) in the apo- and Cu(I)-bound states reveal that the latter possesses a surface-accessible cuprous-ion-binding site located in a dish-shaped region of β-sheet structure. A cuprous ion is transferred under a favourable thermodynamic gradient from ECuC to Sco with no back transfer occurring. The ionization properties of the cysteine residues in the Cys^{86}xxxCys^{90} copper-binding motif of Sco, together with their positional locations identified from an X-ray structure of Sco, suggests a role for Cys^{86} in initiating an inter-complex ligand-exchange reaction with Cu(I)–ECuC. Generation of the genetic knockouts, *Δsco*, *Δecuc* and *Δsco*/*ecuc*, and subsequent *in vivo* assays lend support to the existence of a branched extracytoplasmic copper-trafficking pathway in *S. lividans*. One branch requires both Sco and to a certain extent ECuC to cofactor the Cu_A domain, whereas the other uses only Sco to deliver copper to a cuproenzyme to initiate morphological development.

Key words: copper chaperone, cytochrome *c* oxidase, morphological development, *Streptomyces*.

INTRODUCTION

Copper (Cu) is an essential transition metal ion in biology and is required for the function of many proteins and enzymes involved in processes requiring electron transfer, such as in photosynthesis and respiration, as well as in the catalytic oxidation of various substrates. The reversible Cu(I)/Cu(II) redox couple, crucial for biological function, also makes Cu toxic if not maintained in a tightly bound state in intracellular compartments due to Cu(I) being complicit in Fenton-like chemistry and by interfering in [Fe–S] protein assembly [1]. To avoid such deleterious effects, Cu-trafficking pathways in eukaryotic and prokaryotic organisms are operative. Central to these pathways are Cu metallochaperones delivering Cu to apo-forms of Cu-requiring proteins and enzymes or to membrane transporters that act to efflux Cu across the cell membrane to maintain homoeostasis [2–4]. Insight into how Cu transfer is facilitated between proteins has been demonstrated through NMR solution studies [5–9]. The current understanding is that transient protein–protein interactions expedite metal–ligand exchange reactions without the dissociation of the metal to the bulk solvent, ensuring that the potentially toxic cargo always remains secure.

The biogenesis of the Cu/haem aa_3-type CcO (cytochrome *c* oxidase) in aerobic organisms involves a Cu-trafficking pathway utilizing Cu metallochaperones [4]. CcO is an essential enzyme in aerobic respiration and is responsible for the reduction of molecular oxygen to water, utilizing two Cu centres in this reduction process: the dinuclear Cu_A site in CcO subunit II and the Cu_B site in CcO subunit I [10]. In eukaryotes, the Cu metallochaperone Cox17 mediates Cu(I) transfer to the membrane-tethered Cox11 and Sco1 proteins which reside in the inter-membrane space of mitochondria [11]. Cox11 is implicated in Cu_B site assembly [12,13] and Sco1 acts to metallate the dinuclear Cu_A site [14–16]. In prokaryotes, the assembly of the Cu_A site in aa_3-type CcO is less clear [17]. Cox17 is not present in prokaryotic genomes, but Sco-like proteins have been ubiquitously identified and characterized [17]. In certain bacteria, a gene has been identified which encodes for a membrane-attached protein with a $H(M)X_nMX_{21/22}HXM$ Cu-binding motif (Figure 1) [9,18,19]. The genes encoding these proteins are often located directly up- or down-stream of a gene encoding a Sco-like protein, and a role as a Cu(I) metallochaperone, possibly in a similar manner to the eukaryotic Cox17, was initially inferred [18]. Subsequent *in vitro* experiments with PCu_AC (periplasmic Cu_A chaperone) from *Thermus thermophilus* have revealed direct Cu(I) transfer to the Cu_A site of CcO in the presence of apo-Sco [9]. This was interpreted as Sco acting as a thiol-disulfide reductase, maintaining the cysteine residues in the apo-Cu_A site in a reduced form to facilitate Cu(I) delivery from PCu_AC. Recent, *in vivo* studies in *Rhodobacter sphaeroides* cannot, however, reconcile PCu_AC with a significant role in directly metallating the Cu_A site [20], nor incidentally for PcuC (a PCu_AC homologue) in *Bradyrhizobium japonicum* [19].

The genome sequence of the Gram-positive bacterium *Streptomyces lividans* 1326 has recently been determined [21]. This *Streptomyces* strain has a distinct dependence on Cu ions to stimulate morphological development and antibiotic production [22–26]. Recently, we have used a combination of *in vivo* and *in vitro* studies to present convincing evidence that a plasma membrane-tethered extracytoplasmic Sco protein in *S. lividans* (SLI4214; Sco^{Sl}) acts not as a thiol-disulfide reductase, but as a Cu(II)-metallochaperone, responsible under low [Cu] for the aa_3-type CcO activity and initiating a morphological development

Abbreviations: BCA, bicinchoninic acid; BCS, bathocuprione disulfonate; CcO, cytochrome *c* oxidase; ECuC, extracytoplasmic copper chaperone; PCu_AC, periplasmic Cu_A chaperone; SFM, soya flower mannitol; TMPD, *N*,*N*,*N*′,*N*′-tetramethyl-*p*-phenylenediamine; WT, wild-type.

[1] To whom correspondence should be addressed (email jworrall@essex.ac.uk).

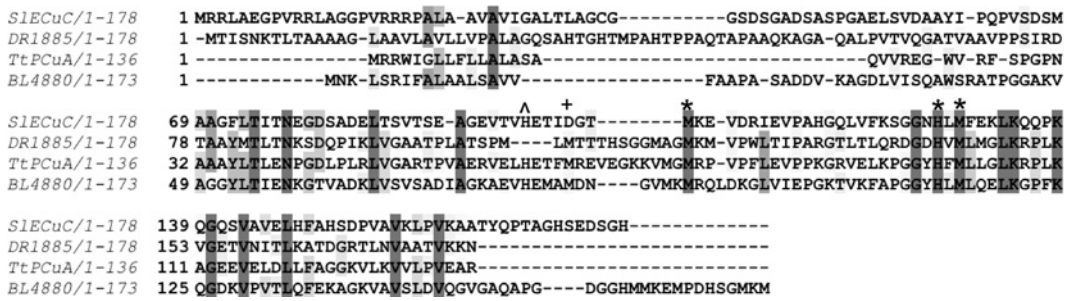

Figure 1 Sequence alignment of *S. lividans* ECuC (SlECuC) with other known bacterial Cu chaperones with a H(M)X_nMX_{21}HXM motif, from *Deinococcus radiodurans* (DR1885), *T. thermophilus* (TtPCuA) and *B. japonicusm* (BL4880)

Completely and partially conserved residues are boxed from dark to light respectively. The MX_{21}HXM part of the motif, conserved across each species, is indicated with a *, with the first residue in the motif, a histidine for ECuC, TtPCuA and BL4880 (^), and a methionine (+) for DR1885.

switch in the life cycle, two unlinked functions [26]. The two genes immediately downstream of the *sco* gene reveal features that suggest involvement in Cu handling and trafficking, with *SLI4213* having a HX_6MX_{21}HXM motif (Figure 1) and the *SLI4212* gene, encoding a putative integral membrane transporter with Cu-binding CopC- and CopD-like domains [27]. This operon structure suggests that a source of Cu(I) for SLI4213 in the extracytoplasmic environment is via SLI4212, which could then be trafficked to enzymes or other chaperones as required. In some Gram-positive bacteria, e.g. *Bacillus subtilis*, no gene encoding a protein with a H(M)X_nM$X_{21/22}$HXM has been identified, and the metallation of the Cu_A site of CcO is inferred to be facilitated by a Cu(II)–Sco interaction [28,29]. In *S. lividans* and other streptomycetes the role and functional relationship with Sco and/or CcO of an extracytoplasmic PCu_AC-like protein has yet to be explored. To extend on our previous studies where we have shown that Sco^{Sl} functions to (i) metallate the Cu_A site of CcO, and (ii) initiate a development switch [26], in the present study we specifically address whether an extracytoplasmic Cu-trafficking pathway exists between Sco^{Sl} and the *SLI4213* gene product. On the basis of its extracytoplasmic location and our Cu-binding studies reported herein, we refer to the SLI4213 protein as ECuC (extracytoplasmic copper chaperone). Using a combination of structural and biochemical studies we show that Cu(I) is transferred in a unidirectional manner from ECuC to Sco^{Sl}. Our analysis suggests that a transient electrostatic complex is formed, with Cu(I) transfer proceeding via a ligand-exchange mechanism with Cys^{86}, part of the Cys^{86}xxxCys^{90} Cu-binding motif in Sco^{Sl}, having an important role. *In vivo* studies using genetic knockouts reveal that under low exogenous Cu concentrations, morphological development is independent of ECuC, but CcO activity is decreased relative to the WT (wild-type) *S. lividans* 1326 strain, implying a co-ordinated role as a Cu donor to Sco^{Sl} in maturation of the Cu_A site in CcO.

MATERIALS AND METHODS

Cloning and overexpression of ECuC in *Escherichia coli*

Bioinformatic analysis predicted the gene product of *SLI4213* to contain an N-terminal TAT pathway signal peptide (http://www.compgen.org/tools/PRED-TAT), and an SPII cleavage site and lipobox (LAGC) just upstream of Cys^{37}, thus suggesting that the *SLI4213* product is a lipoprotein (http://www.cbs.dtu.dk/services/LipoP/, http://bioinformatics.biol.uoa.gr/PRED-LIPO, http://signalfind.org/tatlipo.html). To facilitate the overexpression and to ensure enhanced solubility of the purified product, an N-terminal-truncated *SLI4213* gene encoding amino acid residues 42–178 of ECuC was amplified from *S. lividans* 1326 genomic DNA (*S. lividans* 66, stock-number 1326, John Innes Collection) and ligated into the NdeI and HindIII restriction sites of a pET28a vector (Novagen) to create an N-terminal His_6-tagged construct for overexpression in *E. coli*. ECuC was overexpressed in *E. coli* strain BL21(DE3) cells starting from overnight pre-cultures [2 ml of 2×YT and 2 μl of kanamycin (50 mg/ml), 37 °C] that were subsequently used to inoculate 750 ml of medium in 2 litre flasks. At a D_{600} of 0.6, IPTG (Melford) was added to a final concentration of 1 mM and the temperature was decreased to 25 °C. Cells were harvested after 16 h at 3860 ***g*** and lysed using an EmulsiFlex-C5 cell disrupter (Avestin) followed by centrifugation at 38724 ***g*** for 20 min at 4 °C. The clarified supernatant was loaded on to a 5 ml Ni-NTA (Ni^{2+}-nitrilotriacetate) Sepharose column (GE Healthcare) equilibrated with Buffer A [50 mM Tris/HCl, 500 mM NaCl and 20 mM imidazole (pH 8.0)] and eluted with a linear imidazole gradient using Buffer B (Buffer A with 500 mM imidazole). A single peak at ~22 % Buffer B was eluted from the column and fractions were pooled and dialysed overnight at 4 °C against Buffer C [50 mM Tris/HCl, 150 mM NaCl and 1 mM EDTA (pH 8.0)]. Concentrated protein was loaded on to a G75 Sephadex column (GE Healthcare) equilibrated with Buffer C. Fractions eluting in the major peak of the G75 column were analysed by SDS/PAGE (15 % gel) and those deemed of good purity were concentrated and stored at −20 °C until required. ESI–MS using a Micromass Quattro Ultima triple quadrupole instrument operating in the positive-ion detection mode was used to determine the mass of the purified samples, with individual proteins first desalted and exchanged into 1 M ammonium acetate followed by a 1:20 dilution with a 50 % methanol and 1 % formic acid solution.

Overexpression and purification of Sco^{Sl}

The overexpression of the N-terminal-truncated WT Sco^{Sl} and the C86A, C90A and H176A mutants were carried out as described previously [26,30]. The purified proteins consist of residues 24–216.

Generation of the Δ*ecuc* and Δ*sco*/*ecuc* mutants of *S. lividans* 1326

The agar media SFM (soya flower mannitol), R5 (complex medium) and Difco nutrient agar were prepared according to

Kieser et al. [31]. Antibiotics were used in the following final concentrations: 50 μg/μl apramycin and 5–20 μg/μl thiostrepton. Agar plates were incubated at 30 °C and spore stocks were obtained from cultures grown on SFM plates and stored in 20 % glycerol at − 20 °C. The ECuC mutant (Δ*ecuc*) and the double mutant lacking both ECuC and Sco (Δ*sco*/*ecuc*) were isolated essentially according to the protocol described previously [26]. In the Δ*ecuc* mutant, nucleotides + 21 to + 500 of the *SLI4213* ORF were replaced by a 62-nt scar of the lox recombination site including two XbaI sites. In the double mutant Δ*sco*/*ecuc*, *SLI4214* from nucleotide + 33 and *SLI4213* up to nucleotide + 500 were replaced by the Lox-scar. Both mutants were analysed by PCR to confirm the loss of the gene(s).

In vivo CcO assay

The *in vivo* CcO activity was visualized with TMPD (*N*,*N*,*N*′,*N*′-tetramethyl-*p*-phenylenediamine) as a substrate essentially as described previously [26,32,33]. Each strain was spotted on Difco nutrient agar plates (10 μl containing 1000 spores) and incubated for 24–30 h at 30 °C. Mycelium spots were fixed with a light spray of 0.3 % agarose in water and overlaid with 10 ml of a 25 mM phosphate buffer (pH 7.4) solution containing 20 % ethanol, 0.6 % agarose, 1 % sodium deoxycholate and 10 mg of TMPD. CcO activity was recorded by taking digital images every 30 s for 5–10 min. The ImageJ software (NIH) was used to calculate average pixel intensities of the Indophenol Blue-stained mycelium. After correction for background reading, the data were multiplied by − 1 and plotted as arbitrary units against time.

UV–visible and CD spectroscopies

Concentrations of all apo-proteins were determined by UV–visible spectroscopy (Varian Cary 50 UV–visible spectrophotometer) using molar absorption coefficients (ε) at 280 nm of 2980 $M^{-1}\cdot cm^{-1}$ for ECuC, 14565 $M^{-1}\cdot cm^{-1}$ for Sco^{Sl} and the H176A mutant, and 14440 $M^{-1}\cdot cm^{-1}$ for the C86A and C90A mutants of Sco^{Sl} [34]. Protein samples (20 μM) for CD analysis were exchanged into 10 mM potassium phosphate and 50 mM potassium fluoride and far UV-CD spectra were recorded between 260 and 175 nm at 20 °C on an Applied Photophysics Chirascan CD spectrophotometer equipped with a thermostatic cell holder. CD spectra were analysed using DichroWeb [35].

Competition assays to determine Cu(I)-binding affinities

CuCl (Sigma) was dissolved under anaerobic conditions (DW-Scientific anaerobic chamber) in 10 mM HCl and 500 mM NaCl. The Cu(I) concentration was determined spectrophotometrically by step-wise addition to a known concentration of the Cu(I)-specific bidentate chelator BCA (bicinchoninic acid) using an ε at 562 nm of 7900 $M^{-1}\cdot cm^{-1}$ for $[Cu(BCA)_2]^{3-}$. Protein samples were prepared anaerobically in 10 mM Mops (pH 7.5) and 200 mM NaCl, and, in the case of WT and the H176A mutant of Sco^{Sl}, cysteine residues were reduced by overnight incubation in the presence of 5 mM DTT followed by desalting using a PD-10 column (GE Healthcare). Competition assays were set up anaerobically with either BCA or BCS (bathocuprione disulfonate) (Sigma). Increasing protein concentrations (0–50 μM) were added to solutions of $[Cu^{I}L_2]^{3-}$ of defined molar ratio L:Cu(I)$\geqslant$3, creating a series of individual solutions with constant $[Cu^{I}]$ and [L] and various [protein]. Samples were left for ∼1 h and the transfer of Cu(I) from the $[Cu^{I}L_2]^{3-}$ complex to the protein was determined by measuring the absorbance of the $[Cu^{I}L_2]^{3-}$ complex spectrophotometrically for L = BCA at 562 nm (ε = 7900 $M^{-1}\cdot cm^{-1}$) [36] and L = BCS at 483 nm (ε = 13 000 $M^{-1}\cdot cm^{-1}$) [37]. By interchanging L, assays favouring competitive or non-competitive Cu(I) binding could be set-up, which for the latter led to an estimate of the binding stoichiometry. The dissociation constant for Cu(I) [$K_d(Cu^{I})$] was determined from competitive assays by assuming the following reaction (eqn 1):

$$\text{apo} - \text{P} + \text{CuL}_2 \leftrightarrow \text{Cu(I)} - \text{P} + 2\text{L} \quad (1)$$

where P is protein, and by using eqn (2):

$$K_d\beta_2 = \frac{([\text{apo} - \text{P}]_{tot}/[\text{M} - \text{P}]) - 1}{\{([\text{L}]_2/[\text{ML}_2]) - 2\}[\text{ML}_2]} \quad (2)$$

where [L] is the total ligand concentration (BCA or BCS) and the overall formation constant (β_2) is $10^{17.2}$ M^{-2} for $[Cu(BCA)_2]^{3-}$ and $10^{19.8}$ M^{-2} for $[Cu(BCS)_2]^{3-}$ [36,38]. Assays were performed in triplicate and the $K_d(Cu^{I})$ value for a series was initially calculated for each individual solution and then averaged.

Fluorescence spectroscopy

Fluorescence spectroscopy was carried out on a LS 50B fluorimeter (PerkinElmer), thermostatically controlled at 20 °C. Tryptophan fluorescence emission spectra of WT Sco^{Sl} and mutants were collected between 300 and 400 nm following excitation at 295 nm. The excitation slit and the emission slit were set at 5 nm.

Determining the pK_a values of cysteine residues

Reduced apo-proteins (∼300 μM) were prepared in an anaerobic chamber in 5 mM Mops (pH 7.5) and 25 mM KCl, together with a series of mixed buffer systems containing 10 mM each of potassium acetate, Mes, Mops and Tris, and 200 mM NaCl, with the pH of each solution individually adjusted in increments of 0.5 from pH values of 3–10. Reduced protein was added to each buffered solution to give a final concentration of 30 μM and the ε at 240 nm (ε_{240}) was determined spectrophotometrically in a sealed quartz cuvette and plotted as a function of pH. Models describing one (eqn 3) or two (eqn 4) non-interacting macroscopic ionizations were used to determine pK_a values of the cysteine residues (pK_{Cys}):

$$\varepsilon_{240} = \varepsilon_0 + \frac{\Delta\varepsilon 10^{\text{pH}-\text{p}K_a}}{1 + 10^{\text{pH}-\text{p}K_a}} \quad (3)$$

$$\varepsilon_{240} = \varepsilon_0 + \frac{\Delta\varepsilon 10^{\text{pH}-\text{p}K_{a1}} + \Delta\varepsilon_2 10^{2\text{pH}-\text{p}K_{a1}-\text{p}K_{a2}}}{1 + 10^{\text{pH}-\text{p}K_{a1}} + 10^{2\text{pH}-\text{p}K_{a1}-\text{p}K_{a2}}} \quad (4)$$

where ε_o is the extinction of the thiol form and $\Delta\varepsilon$ is the difference between the molar absorption coefficient of a thiol and thiolate form. The pK_a values reported are an average of multiple datasets and the error reported is the S.D.

Crystallization and structure determinations

Crystals of Cu(I)–ECuC, apo-ECuC and Sco C90A were grown using the hanging-drop vapour diffusion method at 20 °C. Equal volumes of protein solution at a concentration of 15–20 mg/ml were mixed with an equal volume of reservoir solution containing 30 % PEG-MME 2000 and 0.1 M potassium thiocyanate for

Table 1 Crystallographic data collection and processing statistics for *S. lividans* ECuC and Sco C90A structures

Values in parentheses refer to the outermost resolution shells.

Dataset	Cu(I)–ECuC (SAD)	Cu(I)–ECuC (high-resolution)	Apo-ECuC	Apo-Sco^{SI} C90A
Wavelength (Å)	0.9163	0.9163	1.20	0.98
Resolution (Å)	34.6–2.30	27.3–1.48	34.1–1.70	35.7–1.40
Space group	$P2_12_12_1$	$P2_12_12_1$	$P2_12_12_1$	$P3_2$
Unit cell (Å)	44.4, 47.9, 50.1	44.5, 47.8, 50.0	43.6, 47.7, 49.0	41.2, 41.2, 76.6
Unique reflections	5047	17951	44652	28622
Completeness (%)	99.3 (99.5)	98.1 (98.8)	98.0 (89.5)	99.8 (98.5)
R_{merge}	0.045 (0.068)	0.056 (0.482)	0.087 (0.445)	0.067 (0.66)
Mn(I/sd)	53.4 (39.2)	9.5 (2.2)	8.8 (1.9)	10.1 (2.1)
Redundancy	20.6 (23.1)	3.3 (3.4)	3.9 (2.4)	3.3 (2.4)
Anomalous redundancy	11.2 (12.2)	-	-	-
R_{cryst}	-	0.185	0.183	0.131
R_{free}	-	0.227	0.233	0.185
ESU based on ML (Å)	-	0.057	0.080	0.044
RMSD				
Bond lengths (Å)	-	0.016	0.015	0.017
Bond angles (°)	-	1.8	1.8	1.9
Ramachandran favoured (%)	-	95.0	95.2	98.1
Wilson *B*-factor (Å^2)	23.5	26.6	29.3	17.6
PDB accession number	-	3ZJA	3ZK0	4BPY

Cu(I)–ECuC, 31 % PEG 8000, 0.1 M sodium cacodylate (pH 6.5) and 0.2 M sodium acetate for apo-ECuC, and 28 % PEG 4000 and 0.05 M sodium acetate (pH 4.5) for Sco C90A. Crystals suitable for diffraction studies grew within 14 days. A single crystal was transferred to a cryoprotectant solution containing the respective reservoir solution and 10–20 % glycerol before flash-cooling by plunging into liquid nitrogen. Crystallographic data were measured at beamlines I04-1 [Cu(I)–ECuC], I02 (apo-ECuC) and I24 (Sco C90A) of the Diamond Light Source, using X-ray wavelengths of 0.9163, 1.20 and 0.98 Å (1 Å = 0.1 nm) respectively and a Pilatus 6M detector (Dectris). Data were indexed using iMosflm [39] before scaling and merging using Scala [40] in the CCP4i suite. The structure of Cu(I)–ECuC was solved by Cu-SAD phasing in PHENIX [41] using the single intrinsic Cu atom. A high redundancy dataset (anomalous multiplicity of 11.2), measured to 2.3 Å resolution was used to locate the Cu atom and, following density modification, to produce an electron-density map into which a partial model could be built. Extension of the resulting phases to a 1.48 Å resolution dataset resulted in a clear electron-density map from which automatic model building using Buccaneer [42] and ARP/wARP [43] was successful in building 110 residues of the protein sequence. At this stage, the Cu ion was built into a 16σ peak in the $F_o - F_c$ difference map. Subsequent refinement of the structure was carried out using Refmac5 [44] in the CCP4i suite, with model building between refinement cycles in Coot [45], extending the model to include residues 50–164. Riding hydrogen atoms were added when refinement of the protein atoms had converged and individual anisotropic *B*-factors were refined. The structure of apo-ECuC, to a 1.70 Å resolution, was refined using the Cu(I)–ECuC structure, from which the Cu atom had been removed, as a starting model and refined in a similar way except that isotropic *B*-factors were used. Both structures were verified using the Molprobity server [46] and Coot [45]. The Sco C90A structure was solved by molecular replacement using the BALBES server [47] with a search model based on PDB entry 2B7K producing a solution. Model building was initially carried out in ARP/wARP [43] and subsequent refinement and validation as described above. Co-ordinates and structure factors were deposited in the RCSB PDB with accession numbers 3ZJA ,3ZK0 and 4BPY for Cu(I)–ECuC, apo-ECuC and Sco C90A respectively A summary of data and refinement statistics and the quality indicators for all structures reported are given in Table 1.

RESULTS

Cu(I) binding to apo-ECuC causes a large spectral transition in the CD spectrum

From size-exclusion chromatography, ECuC (residues 42–178) eluted at a retention volume consistent with it being a monomer in solution, with a mass determined from ESI–MS of 14694 ± 0.3 Da (predicted 14694 Da after His_6 tag removal). In the UV–visible spectrum no absorption bands in the visible region were present, and only an absorption band in the UV region with a λ_{max} of 275 nm, arising from the presence of a single tyrosine residue in the sequence, was observed. The far-UV CD spectrum reveals a shoulder at ∼230 nm that leads to a trough at ∼200 nm (Figure 2), which is not characteristic of a protein with either α-helical or model β-sheet features, but is instead reminiscent of a spectrum reporting the presence of β_{II}-type sheets. This secondary structure type has been suggested to consist of smaller β-strands that are not ordered or are distorted to one another [48]. Under anaerobic conditions the addition of Cu(I) to ECuC led to significant change in the far-UV CD spectrum that resulted in a positive peak at 200 nm and a trough at ∼235 nm (Figure 2). These features are now indicative of secondary structure dominated by model β-sheet implying that, in solution, ECuC binds Cu(I) causing reorganization of the sheet structure.

Cu(I) binds to *S. lividans* ECuC with subfemtomolar affinity

To explore further the Cu(I)-binding properties of ECuC, the Cu(I)-specific chromogenic bidentate probes BCA and BCS were used under anaerobic conditions. Under the conditions used, addition of increasing amounts of ECuC into $[Cu^I(BCA)_2]^{3-}$ led to a decrease in the absorbance maximum at 562 nm of the $[Cu^I(BCA)_2]^{3-}$ complex (inset of Figure 3A), which when plotted against [ECuC]/[Cu(I)] revealed that ∼1 equivalent of

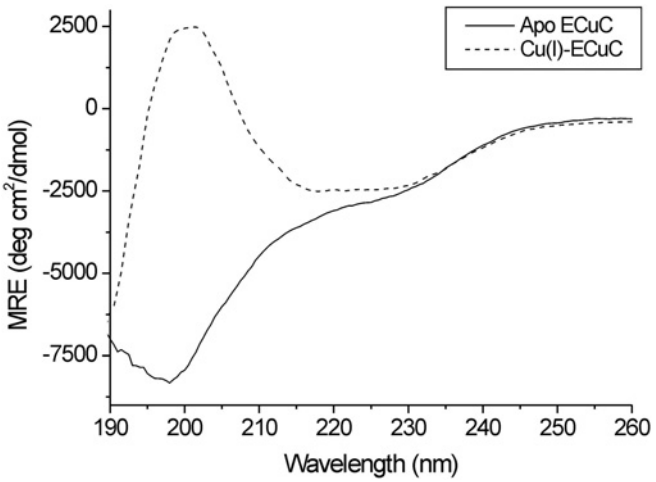

Figure 2 The far-UV CD spectra of *S. lividans* ECuC in the absence and presence of Cu(I)

The apo-protein was incubated under anaerobic conditions with a stoichiometric addition of Cu(I) before measurement at 20 °C. Protein concentration was 20 μM in 10 mM potassium phosphate and 50 mM potassium fluoride (pH 7.5).

Cu(I) is extracted from the $[Cu^{I}(BCA)_2]^{3-}$ complex per monomer of ECuC (Figure 3A). This implies that ECuC binds Cu(I) specifically and that, under the concentrations used, BCA cannot compete with ECuC for Cu(I). In contrast, competition for Cu(I) was observed between ECuC and $[Cu^{I}(BCS)_2]^{3-}$, as indicated from the incomplete bleaching of the absorbance maxima at 483 nm for the $[Cu^{I}(BCS)_2]^{3-}$ complex (inset of Figure 3B). Analysis of these data using eqn (2) with a β_2 of $10^{19.8}$ M^{-2} for $[Cu^{I}(BCS)_2]^{3-}$ gave a $K_d(Cu^{I})$ of 1.9×10^{-16} M, which was used to simulate a fit of the data, shown by the unbroken line in Figure 3(B). Multiple datasets were obtained with various $[Cu^{I}]_{total}$ or [BCS], and an average $K_d(Cu^{I})$ for ECuC reported in Table 2 was obtained. The subfemtomolar affinity of Cu(I) for ECuC is thus in keeping with a putative Cu chaperone role. Addition of Cu(II) to ECuC under aerobic or anaerobic conditions led consistently to the formation of Cu(I)–ECuC.

Structure of the Cu(I)-bound and apo form of ECuC

A single protein molecule was found in the crystallographic asymmetric unit of a crystal of Cu(I)–ECuC, with continuous and well-defined electron density for residues 51–164. The overall structure of Cu(I)–ECuC is shown in Figure 4(A) and consists of a β-barrel-type fold comprising ten β-strands. Analysis of the structure in PDBeFold revealed only one protein with a high structural homology (0.6 compared with 0.27 Q-score for the next hit), indicating that ECuC has a high degree of structural homology with the solution NMR structure of PCu_AC from *T. thermophilus*. A single Cu site is located in a small dish-shaped region of β-structure on the exterior of the β-barrel involving β-sheets 4, 5 and 8 (Figure 4B). The Cu(I) ion is co-ordinated by four residues, comprising His^{98} (β-sheet 4), Met^{105} (β-sheet 5) and two residues from β-sheet 8, His^{127} and Met^{129} (Figure 4B). The bond lengths between the ligands and Cu(I) ion are reported in Table 3, along with the bond angles, which are suggestive of a distorted tetrahedral geometry. An X-ray fluorescence edge scan of a Cu(I)–ECuC crystal gave a shoulder at ~8980 eV that is distinctly different in shape and energy (8984 eV) to digonally or trigonally co-ordinated Cu(I) species and also in energy (8988–8990 eV) to tetrahedral Cu(II) species (Supplementary Figure S1 at http://www.biochemj.org/bj/459/bj4590525add.htm). The two methionine Cu ligands are solvent-exposed with their Cγ atoms present at the protein surface, whereas the two histidine residues are buried and act to 'push' the Cu atom up and away from the dish-shaped region (Figure 4B). Neither of the two methionine ligands have any further interactions, whereas one of two histidine ligands, His^{98}, has a hydrogen bond from its Nε2 atom to a water molecule.

The crystal structure of apo-ECuC also comprises one molecule in the crystallographic asymmetric unit, with well-defined electron density visible for residues 48–164. Superimposition of the Cu(I) and apo-structures, as shown in Figure 4(C), does not reveal any major differences, with an RMSD in Cα positions of 0.4 Å. Subtle differences are noted, however, and are confined to the end of β-sheet 4 and to a slight lengthening of β-sheet 5 in the apo-structure (Figure 4C). In the absence of Cu(I) the ligand residues are now considerably more dynamic, with multiple side-chain alternative conformations being modelled into the electron-density map (Figure 4D). The exception being His^{98}, where a single imidazole ring conformer is modelled which is rotated 90° relative to its orientation in the Cu(I)–ECuC structure and the hydrogen-bond interaction through the Nε2 atom to a water molecule remains. The extent of the changes in side-chain orientations between the Cu(I)-bound ECuC and apo-ECuC are indicated from the superimposition of the Cu site in Figure 4(E).

Cu(I) binds to Sco^{Sl} with a higher affinity than to ECuC

Sco^{Sl} has been previously reported to bind a Cu(II) ion with high affinity ($K_d > 10^{-12}$ M) and it has subsequently been shown that it is the cupric oxidation state that is required for its role in the Cu-dependent morphological development switch of *S. lividans* and in metallating CcO [26]. Before assessing whether Cu transfer between ECuC and Sco^{Sl} can occur, Cu(I) binding to Sco^{Sl} has been investigated. At pH 7.5, addition of increasing amounts of reduced apo-Sco^{Sl} into $[Cu^{I}(BCA)_2]^{3-}$ revealed that BCA cannot compete with apo-Sco^{Sl} for Cu(I) under the concentrations used and one Cu(I) ion binds per monomer of Sco^{Sl} (Figure 3C). Using $[Cu^{I}(BCS)_2]^{3-}$, competition for Cu(I) between Sco^{Sl} and BCS is observed (Figure 3D). Analysis of these data using eqn (2) with a β_2 of $10^{19.8}$ M^{-2} for $[Cu^{I}(BCS)_2]^{3-}$ gave a $K_d(Cu^{I})$ of 6.5×10^{-17} M, which was used to simulate a fit of the data, shown by the unbroken line in Figure 3(D). Multiple datasets were obtained with various $[Cu^{I}]_{total}$ or [BCS] and an average $K_d(Cu^{I})$ for reduced apo-Sco^{Sl} at pH 7.5 is reported in Table 2, indicating an ~4-fold higher affinity for Cu(I) than ECuC.

Structure of the C90A mutant of Sco^{Sl}

The overall structure of the C90A mutant of Sco^{Sl} is shown in Figure 5(A). All efforts to crystallize the WT protein in the presence and absence of Cu were unsuccessful. The C90A mutant has been previously studied in respect to the kinetics and mechanism of Cu(II) capture by the Cys^{86}xxxCys^{90} motif in Sco^{Sl} [30]. A single protein molecule was found in the crystallographic asymmetric unit of a crystal of Sco^{Sl} C90A. The monomeric fold consists of five α-helices one 3_{10} helix and eight β-strands, with strands β4, β5, β7 and β8, and helices α1, α4 and α5 forming the core of a typical thioredoxin fold (Figure 5A). Typical of other Sco proteins, additional secondary structure is inserted at the N-terminus. A long twisted β-strand (β1) is present, which is either absent or considerably shorter in other known structures of Sco proteins and wraps around the core β7 and β8 strands

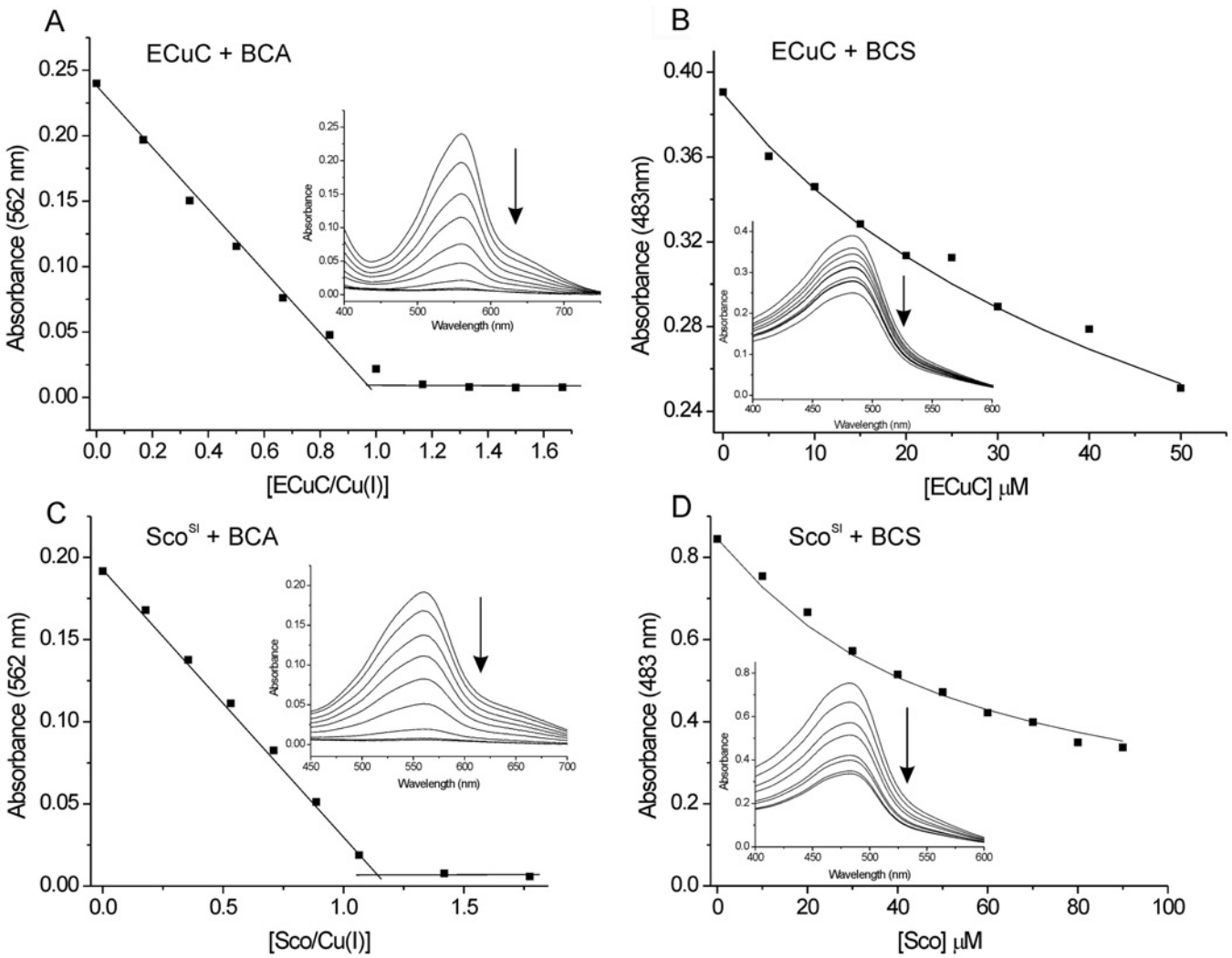

Figure 3 Determination of the Cu(I) stoichiometry and $K_d(Cu^I)$ for *S. lividans* ECuC and Sco^{SI} at pH 7.5 using the chromogenic probes BCA and BCS

(**A**) Plot of the absorbance change at 562 nm in the $[Cu^I(BCA)_2]^{3-}$ spectrum (inset) as a function of [ECuC]:[Cu(I)]. No competition between ECuC and BCA is observed on the basis that the absorbance at 562 nm decreases to zero with increasing amounts of ECuC. The intersections of the lines at the start and end of the titration indicate a stoichiometry of Cu(I) binding to ECuC of $\sim$1. Conditions used: 0–50 μM [ECuC], 30 μM $[Cu^I]_{total}$ and 120 μM [BCA]. (**B**) Plot of the absorbance change at 483 nm in the $[Cu^I(BCS)_2]^{3-}$ spectrum (inset) under Cu(I)-limiting conditions imposed by $[Cu^I(BCS)_2]^{3-}$ as a competitive probe as a function of [ECuC]. The line through the data points represents a best fit using a $K_d(Cu^I)$ of 1.9×10^{-16} M determined using eqn (2). Conditions used: 0–50 μM [ECuC], 30 μM $[Cu^I]_{total}$ and 120 μM [BCS]. (**C**) Plot of the absorbance change at 562 nm in the $[Cu^I(BCA)_2]^{3-}$ spectrum (inset) as a function of $[Sco^{SI}]$:[Cu(I)]. As for ECuC, no competition with BCA is observed and a stoichiometry of Cu(I) binding to Sco^{SI} of $\sim$1 is determined. Conditions used: 0–45 μM $[Sco^{SI}]$, 25 μM $[Cu^I]_{total}$ and 75 μM [BCA]. (**D**) Plot of the absorbance change at 483 nm in the $[Cu^I(BCS)_2]^{3-}$ spectrum (inset) under Cu(I)-limiting conditions imposed by $[Cu^I(BCS)_2]^{3-}$ as a competitive probe as a function of $[Sco^{SI}]$. The line through the data points represents a best fit using a $K_d(Cu^I)$ of 6.5×10^{-17} M determined using eqn (2). Conditions used: 0–90 μM $[Sco^{SI}]$, 65 μM $[Cu^I]_{total}$ and 150 μM [BCS].

of the thioredoxin fold (Figure 5A). Following on from $\beta1$ is the conserved β-hairpin structure ($\beta2+\beta3$) and a 3_{10} helix (Figure 5A). A second insertion of secondary structure on to the thioredoxin scaffold is found between $\beta5$ and $\alpha4$ and consists of the helix $\alpha3$ and the stand $\beta6$ and finally, unique to Sco^{SI}, a short α-helix ($\alpha2$) is inserted between $\alpha1$ and $\beta5$ (Figure 5A). Analysis of the structure using PDBeFold reveals the highest structural homology (0.59 Q-score) with the solution NMR structure of the Sco protein from *T. thermophilus* followed by the Sco proteins from yeast and human (0.54 and 0.53 Q-scores respectively). The electron density is continuous from residues 42–164 and 177–216, with the region between amino acids 165 and 176 having discontinuous electron density and, as a consequence, these 12 residues are not included in the model (Figure 5A). This observation is indicative of a flexible dynamic protein region and is consistent with reports that the loop connecting $\alpha4$ to $\beta7$, referred to as the 'Sco-loop', is dynamic and flexible and thus gives rise to disorder in the C90A crystal. Within this missing 12-residue stretch, His^{176} is located, a residue which has been previously shown in Sco^{SI} to act as a co-ordinating ligand to the Cu(II) ion bound to the CxxxC motif [26].

An unexpected feature of the C90A structure is that the electron density for the Cys^{86} side chain is suggestive of a modification (Figure 5B). We modelled a sulfinic and sulfonic acid functional group at this position and found that the former, with two oxygen atoms, provides the best fit to the electron density (Figure 5B). ESI–MS of the C90A sample before crystallization gave a mass as expected and therefore this oxidizing modification must have either taken place over time during the crystallization process or possibly in the X-ray beam. As a consequence of this modification, the oxygen atoms of the sulfinic group are able to form hydrogen bonds with the backbone amide of Asp^{88} and Ala^{90} and thus

Table 2 Cu(I) affinities determined at pH 7.5 for ECuC, Sco^{Sl} and Sco^{Sl} variants and pK_{Cys} and $\Delta\varepsilon$ values at 240 nm for the respective Sco^{Sl} proteins

Protein	K_d (Cu^I) (M)	pK_{Cys1}	pK_{Cys2}	$\Delta\varepsilon_1$ ($mM^{-1}\cdot cm^{-1}$)	$\Delta\varepsilon_2$ ($mM^{-1}\cdot cm^{-1}$)
ECuC	$2.0\ (0.2) \times 10^{-16}$	-	-	-	-
Sco^{Sl}	$4.6\ (1.4) \times 10^{-17}$	6.22 (0.11)	8.90 (0.46)	3.2 (0.4)	1.1 (0.1)
C86A	$8.3\ (1.3) \times 10^{-14}$	6.34 (0.32)	-	2.3 (0.2)	-
C90A	$2.8\ (1.3) \times 10^{-16}$	6.54 (0.41)	-	2.7 (0.2)	-
H176A	$1.5\ (0.8) \times 10^{-14}$	6.56 (0.13)	8.90 (0.45)	3.1 (0.1)	2.0 (0.3)

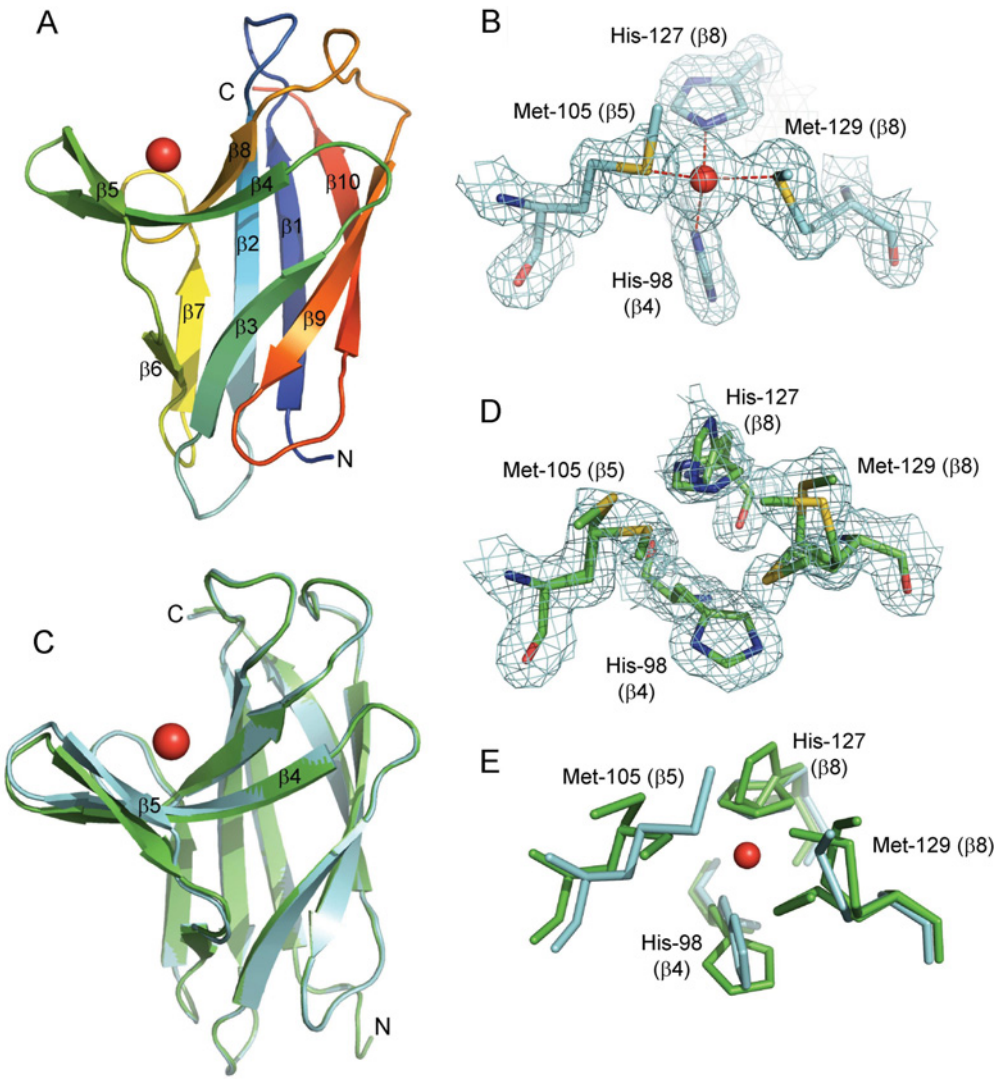

Figure 4 X-ray crystal structure of *S. lividans* ECuC

(**A**) Cartoon representation of Cu(I)–ECuC with the Cu ion shown as a red sphere. The β-strands 1–10 are labelled and the positions of the N- and C-termini are indicated. (**B**) $2F_o - F_c$ electron-density map contoured at 1 σ of the Cu(I)-binding site of ECuC with the ligands to the Cu(I) ion and their β-strand location indicated. (**C**) Superimposition (calculated in the CCP4 suite) of the Cα atoms of the Cu(I)–ECuC structure (cyan) with the apo-ECuC structure (green). The N- and C-termini are indicated as well as the β4 and β5 strands where significant structural changes occur between the two structures. (**D**) $2F_o - F_c$ electron-density map contoured at 1 σ of the Cu(I) site ligands in the apo-ECuC structure with the multiple orientations of the side chains built into the density for each ligand shown. (**E**) Superimposition of the Cu(I)–ECuC and apo-ECuC Cu-binding sites.

serve to add stability to the loop harbouring the CxxxC motif (Figure 5B). In the absence of this modification, it is highly unlikely that the thiol group of Cys^{86} will participate in any hydrogen-bond interactions. A superimposition of the Cys^{86} loop region between different prokaryotic Sco proteins is shown in Figure 5(C), with positional differences in the loop between proteins from different species clearly apparent. The most notable is the position of the cysteine residue in Sco^{Bs} (equivalent to Cys^{90} in Sco^{Sl}) (Figure 5C). In all of the other structures, the second cysteine residue of the CxxxC motif is the second residue in helix α1, whereas in Sco^{Bs} it remains highly solvent-exposed on the loop (Figure 5C). This would appear to be a consequence of the loop length being largest for Sco^{Bs} and shorter among the other species.

Table 3 Bond lengths and angles for the Cu(I) site of *S. lividans* ECuC

(a) Bond length

Bond	Length (Å)
Cu–His^{98} Nδ1	2.15
Cu–Met^{105} Sδ	2.25
Cu–His^{127} Nε2	2.08
Cu–Met^{129} Sδ	2.31

(b) Bond angle

Bond	Angle (°)
His^{98} Nδ1–Cu–Met^{105} Sδ	113.6
His^{98} Nδ1–Cu–His^{127} Nε2	108.3
His^{98} Nδ1–Cu–Met^{129} Sδ	109.9
Met^{105} Sδ–Cu–His^{127} Nε2	109.9
Met^{105} Sδ–Cu–Met^{129} Sδ	115.3
His^{127} Nε2–Cu–Met^{129} Sδ	98.7

Cu(I)–ECuC can transfer Cu to Sco^{Sl}

To assess whether ECuC and Sco^{Sl} can participate in Cu(I) ion transfer with each other, tryptophan fluorescence was used. A single tryptophan residue, Trp^{132}, is present in Sco^{Sl}, whereas ECuC has no tryptophan residues. The crystal structure of Sco^{Sl} C90A reveals that Trp^{132} is located on helix α3 and is within 6 Å of the backbone amide of Cys^{86} (inset of Figure 6A). Binding of either Cu(II) or Cu(I) to the CxxxC motif in Sco^{Sl} leads to a quenching of the tryptophan emission intensity at 330 nm [26], as indicated in Figure 6(A), and thus Trp^{132} serves as a sensitive probe to follow Cu ion binding to Sco^{Sl}. Mixing both apo-proteins in a 1:1 stoichiometry has no effect on the Trp^{132} emission spectrum of Sco^{Sl} over a period of hours (Figure 6B). In contrast, the addition of a stoichiometric equivalent of Cu(I)–ECuC to apo-Sco^{Sl} causes rapid instantaneous quenching in the emission spectrum (Figure 6C and inset) and indicates that Cu is now bound to Sco^{Sl}. As no other source of Cu ions were present in solution, this is clear evidence that Cu is transferred from ECuC to Sco^{Sl}. From the fluorescence quenching it was not possible to identify the oxidation state of the Cu bound to Sco^{Sl} following the transfer. However, no characteristic Cu(II)–Sco^{Sl} absorbance bands were present in the visible spectrum [26] of the mixture and it was therefore concluded that Cu was transferred and remained bound to Sco^{Sl} in the cuprous state. The reverse experiment, whereby Cu(I)–Sco^{Sl} was mixed stoichiometrically with apo-ECuC did not yield an increase in the emission intensity of the tryptophan fluorescence spectrum, which would have be expected to occur if Cu was being transferred from Sco^{Sl} to ECuC (Figure 6D). These results therefore reveal that Cu(I) is transferred in a unidirectional manner from ECuC to Sco^{Sl} and, for transfer to occur, a complex between the two proteins must therefore be formed. Figure 7 shows surface electrostatic maps of Cu(I)–ECuC and Sco^{Sl} C90A where it is apparent that both proteins have a significant overall negative charge (theoretical pI values of 4.8 and 5.0 for ECuC and Sco^{Sl} constructs used respectively). Nevertheless, a complementary charged patch is observed between the region around the Cu(I) site of ECuC and the CxxxC region of Sco^{Sl} (Figure 7).

Two distinct ionization processes for the cysteine residues in the CxxxC motif of Sco^{Sl}

The ionization properties of cysteine thiol groups in Atx1-like metallochaperones that have a CxxC motif have been reported to be important for facilitating metal ion transfer [49,50]. To

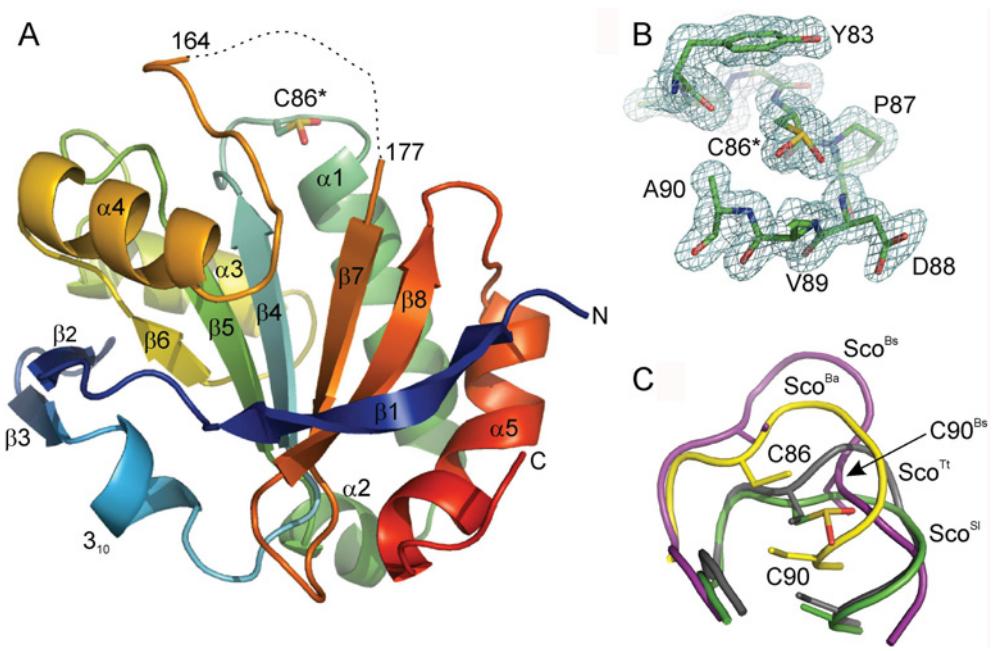

Figure 5 X-ray crystal structure of the C90A mutant of Sco^{Sl}

(**A**) Cartoon representation of Sco^{Sl} with the secondary structure components that make up the fold labelled. The N- and C-termini are indicated and the modified Cys^{86} residue, part of the CxxxC motif, is shown as sticks. The broken line connecting residues 164–177 is to illustrate the 'Sco-loop' that houses His^{176}, a ligand in the Cu-bound form, that is not observable in this crystal structure. (**B**) $2F_o - F_c$ electron-density map contoured at 1 σ of the CxxxC motif illustrating the modified thiol side chain of Cys^{86} and the position of Ala^{90}. (**C**) Superimposition of the loop containing the CxxxC motif of Sco^{Sl} with those in other prokaryotic Sco proteins (Bs, *B. subtilis*; Ba, *B. anthracis*; Tt, *T. thermophilus*). The cysteine residues 86 and 90 (*S. lividans* numbering) for each species are shown as sticks.

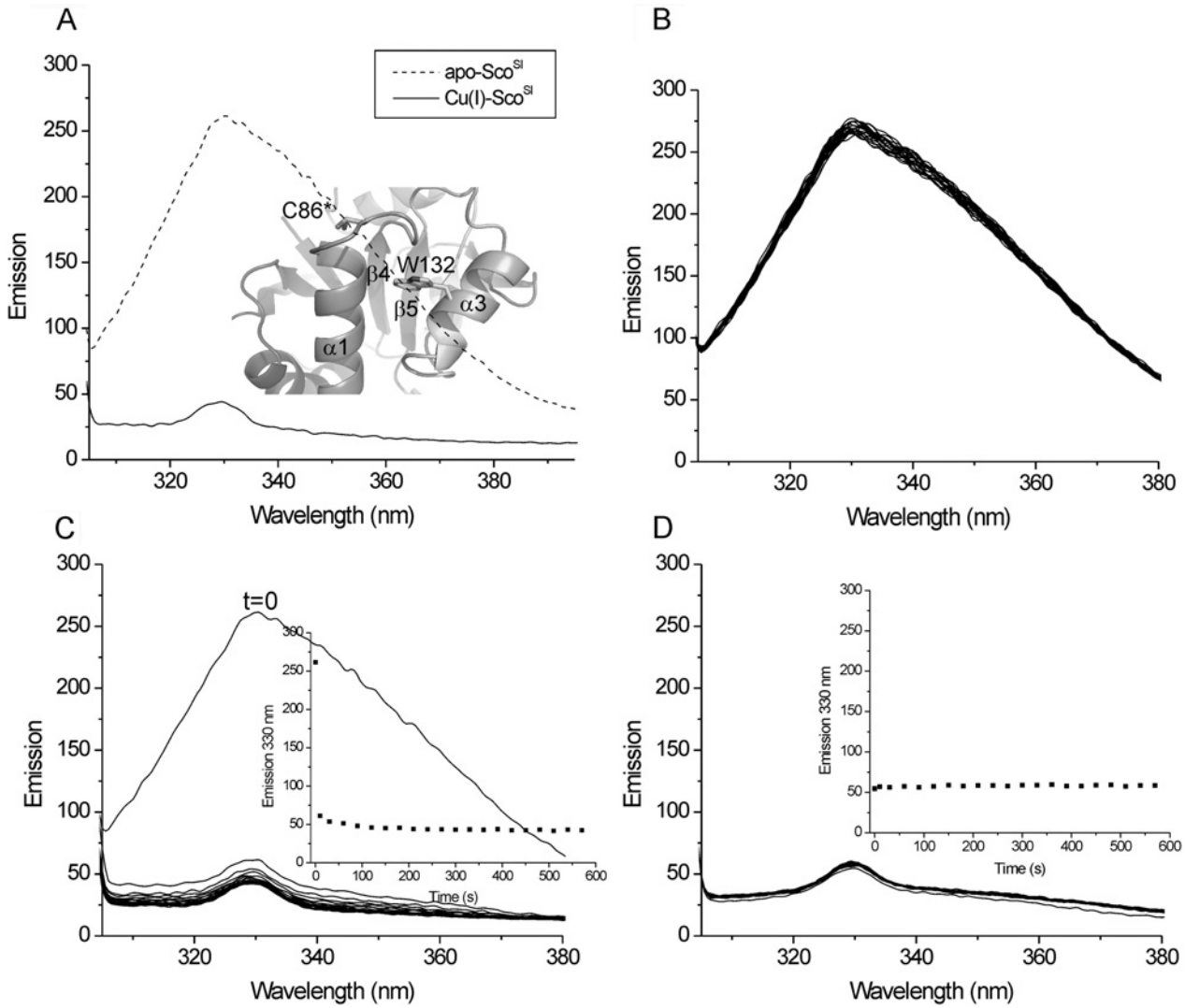

Figure 6 Cu transfer between ECuC and Sco^{Sl} monitored by tryptophan fluorescence

(**A**) Structural location of Trp^{132} in Sco^{Sl} and the quenching of the tryptophan emission spectrum of apo-Sco^{Sl} upon a stoichiometric addition of Cu(I). (**B**) Tryptophan emission spectrum of apo-Sco^{Sl} upon addition of a stoichiometric equivalent of apo-ECuC. (**C**) Quenching of the tryptophan emission of Sco^{Sl} upon incubation of a molar equivalent of Cu(I)–ECuC. Inset, change in tryptophan emission at 330 nm as a function of time after addition of Cu(I)–ECuC. (**D**) Tryptophan emission spectrum of Cu(I)–Sco^{Sl} in the presence of a molar equivalent of apo-ECuC. Inset, change in tryptophan emission at 330 nm as a function of time after addition of apo-ECuC. All experiments were carried out at 20°C, pH 7.5, with excitation at 295 nm.

gain further insight into the transfer of Cu(I) from ECuC to Sco^{Sl}, the pK_a values of the cysteine residues in the CxxxC motif of Sco^{Sl} were determined directly by monitoring the absorbance change at 240 nm as a function of pH (Figure 8A). The data fit best to a model involving two ionizations and the pK_{Cys} and $\Delta\varepsilon$ values are reported in Table 2. For one of the cysteine residues, a pK_{Cys} of 6.3 indicates that at physiological pH the more nucleophilic thiolate form would predominate. The effects on Cu transfer between ECuC and Sco^{Sl} were further assessed through the C86A, C90A and H176A mutants of Sco^{Sl}. All three mutants bound Cu(I) with affinities lower than the WT Sco^{Sl} (Table 2, Figure 8B and Supplementary Figure S2 at http://www.biochemj.org/bj/459/bj4590525add.htm) and for the H176A mutant two ionization processes were detected (Supplementary Figure S3 at http://www.biochemj.org/bj/459/bj4590525add.htm) with the pK_{Cys} values reported in Table 2 very similar to WT Sco^{Sl}. For the C86A and C90A mutants a single ionization process was detected (Figure 8C and Supplementary Figure S3), with pK_{Cys} values for each mutant similar to the lower of the two pK_{Cys} values determined in the WT and H176A proteins (Table 2). Thus removing one of the thiols appears to influence the pK_a of the remaining thiol. We note that the $\Delta\varepsilon$ values determined for the individual cysteine residues in the two cysteine mutants differ (Table 2). This was also observed for the two ionization transitions in the WT and H176A proteins (Table 2). Therefore on the basis of this we propose that the lower pK_{Cys} in the WT Sco^{Sl}, which has the greater $\Delta\varepsilon$, is for Cys^{86}, as the C90A mutant consistently showed a greater $\Delta\varepsilon$, with the higher pK_a assigned to Cys^{90} as the C86A mutant has the smaller $\Delta\varepsilon$. Such an interpretation has also been rationalized for the Hg^{2+} Atx1-like chaperone NmerA [49]. Addition of a stoichiometric amount of Cu(I) to the H176A mutant results in quenching of the Trp^{132} fluorescence, similar to that observed for WT Sco^{Sl}. Quenching is also observed, albeit more slowly, when one equivalent of Cu(I)–ECuC is mixed with the H176A mutant and thus Cu transfer is still viable in the absence of His^{176} in Sco^{Sl}.

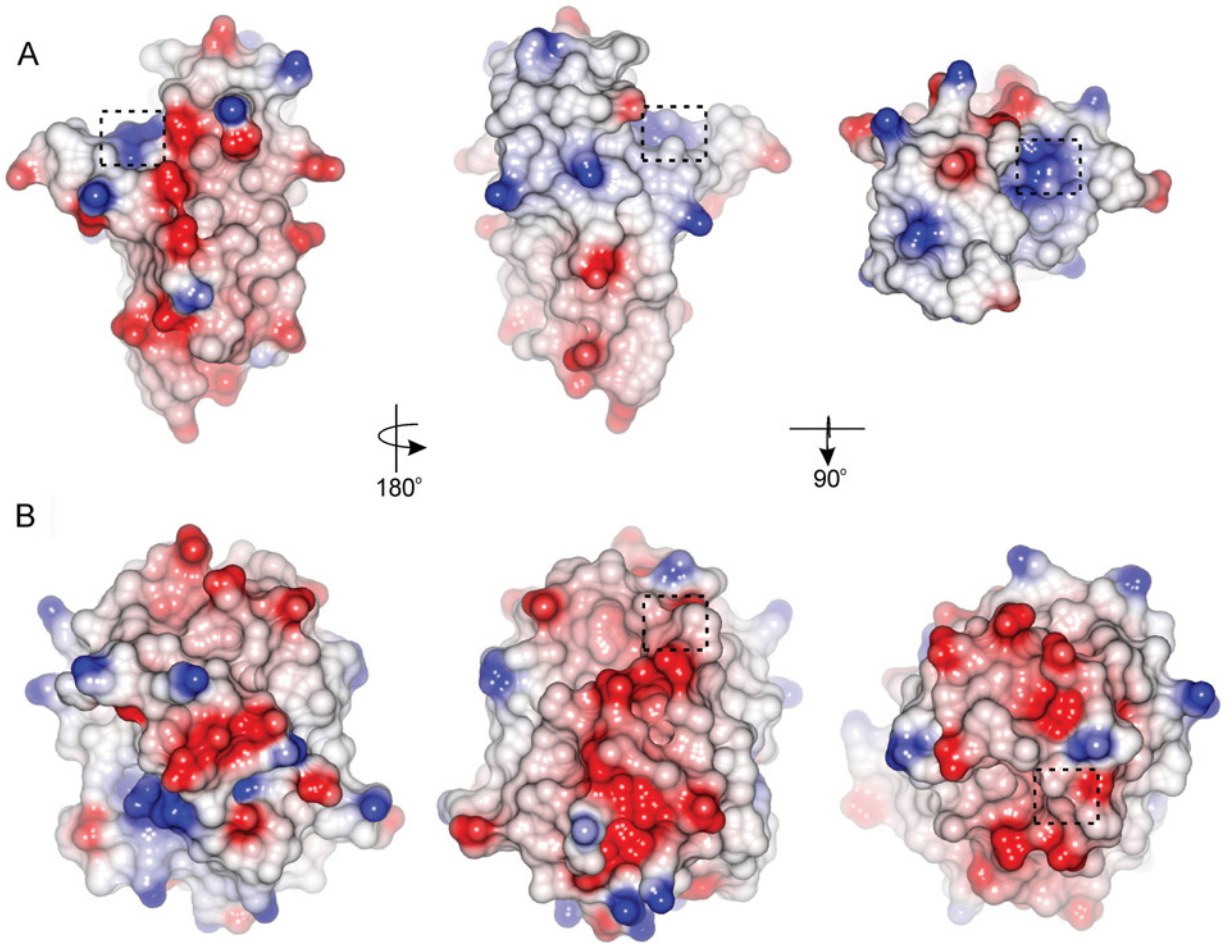

Figure 7 Electrostatic surface representations of (A) Cu(I)–ECuC and (B) Sco^{Sl} (C90A)

Positive charges are indicated in blue and negative charges are indicated in red. The broken box highlights the location of the Cu(I) site in ECuC and the CxxxC motif in Sco^{Sl}.

The situation with the cysteine mutants is complicated by the fact that removal of either cysteine residue alters the fluorescence properties of Cu binding, such that at sub- and stoichiometric Cu concentrations no quenching is observed, despite Cu being bound to the protein [30]. Therefore on mixing Sco^{Sl}/Cu(I)–ECuC under stoichiometric conditions, no quenching was observed and the effect of either cysteine residue on transfer is not determinable.

Morphological development and CcO activity

The above *in vitro* experiments provide strong evidence that Cu(I) can be transferred from ECuC to Sco^{Sl}. To assess the effect of ECuC on morphological development, *ecuc* and *sco*/*ecuc* knockouts were created in *S. lividans* 1326 and the morphological development monitored on R5 medium with various [Cu] (Figure 9A). As previously reported, the *sco* mutant is incapable of switching from vegetative to aerial growth and spore production at low [Cu] [0.1 or 1 μM Cu(II)], with full development restored upon addition of 10 μM Cu(II) (Figure 9A). By contrast the *ecuc* mutant showed full development at low [Cu] comparable with that observed in the WT strain (Figure 9A). The double *sco*/*ecuc* mutant displayed the same 'bald' phenotype (no aerial hyphae growth) as observed for the *sco* mutant at low [Cu], with development fully restored upon addition of 10 μM Cu(II) (Figure 9A). As previously reported, the CcO activity at low [Cu] in the *sco* mutant is close to the background activity measured in a *cco* mutant [26] (Figure 9B). The *ecuc* mutant on the other hand displayed higher CcO activity, ~45% of the WT level, compared with the 20% observed for the *sco* mutant, and the *sco*/*ecuc* mutant showed similar activity levels to the single *sco* mutant (Figure 9B). Together these results suggest that, under low [Cu], Sco^{Sl} is a key protein in the morphological development of *S. lividans*, whereas ECuC has no obvious role, but does appear to have a role together with Sco^{Sl} in CcO maturation.

DISCUSSION

Metallochaperones act in the cell to guide and protect a metal ion while facilitating appropriate partnerships with enzymes or proteins that require the respective metal for function. Sco proteins have received considerable attention in their role as a Cu metallochaperone in both eukaryotic and prokaryotic organisms. In the latter a chaperone role for Sco has been questioned, but our recent studies in *S. lividans* have provided strong evidence to indicate that Sco^{Sl} functions as a Cu metallochaperone involved in the maturation of the Cu_A site in the aa_3-type CcO and furthermore is essential in triggering a morphological development switch [26]. These observations all occur under low [Cu] when it is expected that the cells most efficient chaperone and scavenging systems operate, expediting delivery and trafficking of Cu to meet

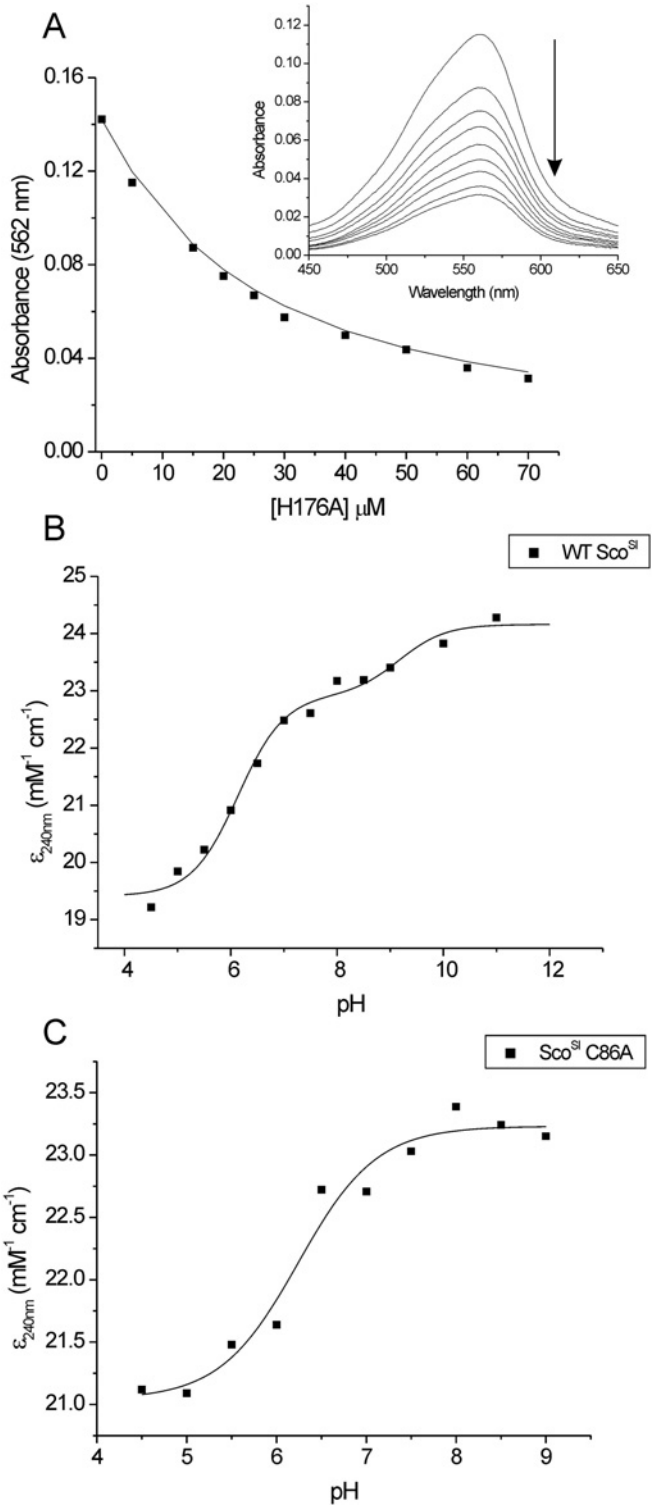

Figure 8 Determination of the $K_d(Cu^I)$ for the H176A mutant and the pK_a values of the cysteine residues in the CxxxC Cu-binding motif of Sco^{Sl}

(**A**) The $K_d(Cu^I)$ for the H176A mutant was determined using $[Cu^I(BCA)_2]^{3-}$ as a competitive probe under Cu(I)-limiting conditions. Inset: the absorbance at 562 nm in the visible spectrum of $[Cu^I(BCA)_2]^{3-}$ decreases upon addition of the H176A Sco^{Sl} variant with a plot of this absorbance change against [H176A] to determine the $K_d(Cu^I)$ using eqn (2). The line through the data points represents a best fit to the data using a $K_d(Cu^I)$ of 9.0×10^{-15} M. Conditions used: 0–50 μM [H176A], 30 μM $[Cu^I]_{total}$ and 120 μM [BCA]. (**B** and **C**) Change in absorbance at 240 nm as a function of pH for WT (30 μM) and the C86A mutant (30 μM) of Sco^{Sl}. For WT the data points are fitted to two ionizations (eqn 4) and for the C86A mutant a single ionization process (eqn 3).

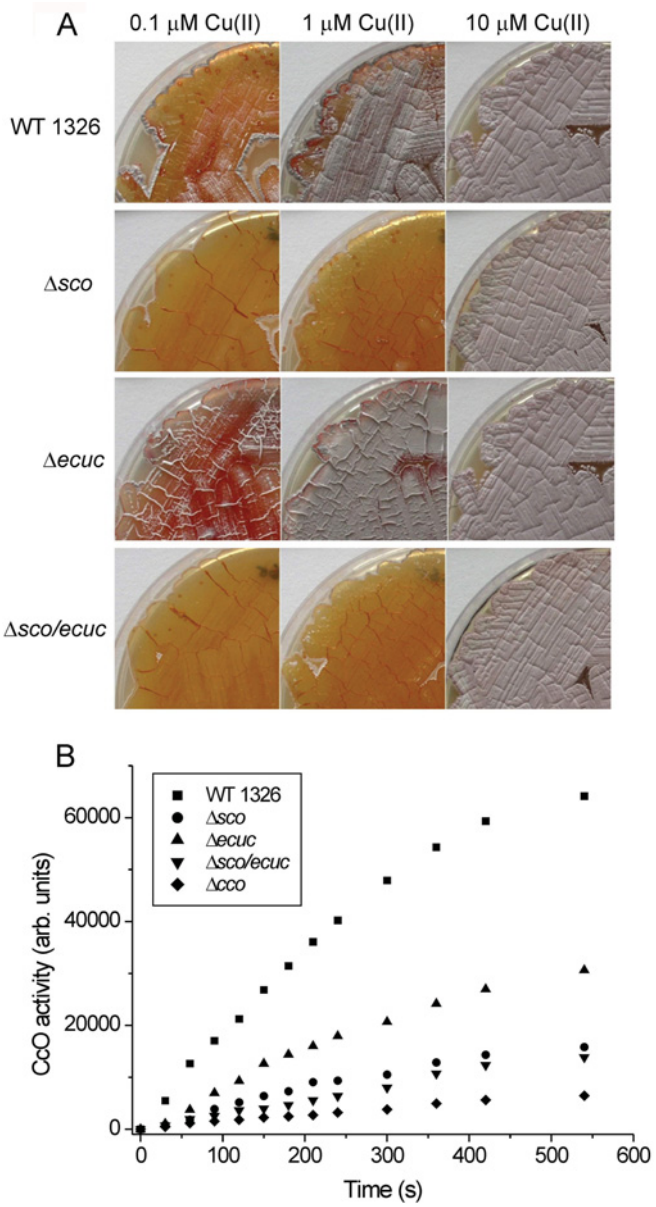

Figure 9 Morphology and CcO activity in *S. lividans* 1326 (WT), Δ*sco*, Δ*ecuc* and the Δ*sco/ecuc* mutant

(**A**) WT and mutants were grown on R5 medium supplemented with 0.1, 1 and 10 μM Cu(II) for 5 days. (**B**) *In vivo* detection of CcO activity with TMPD as substrate as described in [26] and in the Materials and methods section (S.D. varied from 5 % to 16 %).

the metabolic needs of the cell. Sco^{Sl} is secreted in *S. livdians* via the Sec pathway so it is likely to acquire Cu once folded in the extracytoplasmic environment. One possibility for Cu acquisition by Sco^{Sl} is via another chaperone, such as ECuC. The structure of Cu(I)–ECuC reveals a Cu(I)-binding site consisting of Met_2His_2 ligands in a $HX_6MX_{21}HXM$ motif, which, together with the overall protein fold, reveals that ECuC belongs to the PCu_AC family of Cu chaperones. These proteins, which, depending on species, also bind Cu(I) in a Met_3His co-ordination arrangement, are present in the more oxidizing cellular compartments of bacteria, such as the periplasm or in the case of *S. lividans* the extracytoplasmic environment, and utilize methionine ligands in place of the more oxidation-prone cysteine ligands to co-ordinate Cu(I). ECuC is found to co-ordinate Cu(I) in a dish-shaped region with both

methionine ligands solvent-exposed and asides co-ordinating the Cu ion do not participate in further protein interactions. In the absence of Cu(I) the Met_2His_2 ligands are dynamic and small changes in sheet structure in the vicinity of the Cu(I) site were observed (Figure 4). However, whether these are considerable enough to give rise to the CD transition between apo- and Cu(I)-bound is unclear (Figure 2). It is likely that in solution apo-ECuC can access conformations with more altered sheet structure that are not detectable in the crystalline state, and that the CD spectrum may be an average representation of a number of dynamic conformations, which become stabilized on binding Cu(I). The overall charge at the ECuC Cu site with Cu(I) bound is $+1$, and this helps create a positively charged surface patch that will favour Cu transfer to a negatively charged recipient (Figure 7A).

According to the Cu trafficking hypothesis Cu moves from the donor chaperone to the target protein with or against a relatively shallow thermodynamic gradient as defined by K_{Cu}, measured with purified proteins [51,52]. Using the affinity probe BCS, ECuC was determined to have subfemtomolar affinity for Cu(I). Despite inhabiting the extracytoplasmic environment, Sco^{Sl}, in contrast with ECuC, utilizes two cysteine residues and a histidine residue to co-ordinate a Cu(I) ion, with a $K_d(Cu^I)$ ~4-fold higher than ECuC (Table 2). The very high Cu(I) affinities determined for ECuC and Sco^{Sl} are in keeping with other studies on Cu metallochaperones, and thus trafficking between sites is proposed to involve ligand substitution-like mechanisms [38,50,52]. The structure of the C90A Sco^{Sl} protein has a typical Sco-fold with a negatively charged surface patch centred around the loop harbouring the Cys^{86} ligand (Figure 7). Electrostatic complementarity is a hallmark of chaperone–acceptor pairs, and therefore, based on the electrostatics of Sco^{Sl} and Cu(I)–ECuC (Figure 7), a transient chaperone–acceptor complex is likely to occur. Formation of a chaperone–acceptor adduct may initiate a structural change that opens up the metal-binding site of the chaperone and enable ligand invasion by the acceptor. Therefore, coupled with a favourable thermodynamic gradient for Cu(I) transfer from ECuC to Sco^{Sl}, we envisage that, within the complex, Sco^{Sl} initiates a ligand-exchange mechanism enabling Cu to be transferred from ECuC.

To gain further insight into the mechanism of Cu exchange between these two proteins alanine mutations of the Cu ligands in the acceptor Sco^{Sl} were investigated. In all cases, the affinity for Cu(I) in the mutants is decreased compared with WT Sco^{Sl} (Table 2), with two of the mutants, C86A and H176A, having weaker Cu(I) affinity than ECuC. This results in an unfavourable thermodynamic gradient for Cu(I) transfer from ECuC to either of these Sco^{Sl} mutants. Despite this, Cu(I) transfer to the H176A mutant occurs and factors other than the Cu(I) affinity of Sco^{Sl} must play a role. One of these may be the ability to tune the ionization properties of the cysteine residues in the CxxxC Cu-binding motif of Sco^{Sl}. The reactivity of individual cysteine residues in the Atx1 family of metal chaperones with a CxxC motif has been shown to influence not only Cu(I) binding affinities, but also the reaction rates of Cu(I) transfer, and this property is therefore deemed to be an advantage over methionine ligands in Cu(I) trafficking sites [50,53]. On the basis of the differences in the $\Delta\varepsilon_{240}$ values for the single cysteine mutants and the higher Cu(I) affinity for the C90A mutant compared with the C86A mutant (Table 2), we have assigned the lower (acidic) pK_a in WT Sco^{Sl} to Cys^{86}. A higher concentration of the more reactive thiolate form of Cys^{86} at pH 7.5 is also consistent with previous kinetic studies of Cu(II) loading to Sco^{Sl}, where we found that the S(Cys^{86})-to-Cu(II) interaction had a higher degree of covalency than Cys^{90} and, importantly, Cys^{86} acts as the initial Cu(II) capture ligand in a two-step kinetic mechanism [30]. Furthermore, from the C90A Sco^{Sl} structure (Figure 5), the location of Cys^{86} on a loop segment rather than being locked down in helix $\alpha1$ (as would be the case for Cys^{90}) is favourable for conformational sampling by the Cys^{86} side chain within the transient complex. Therefore we propose, in trafficking Cu(I) from ECuC to Sco^{Sl}, that a transient electrostatic complex is formed, in which Cys^{86} carries out the initial nucleophilic attack (ligand substitution) on the Cu(I) ion bound in the ECuC site, with subsequent ligand exchange occurring to form the Sco^{Sl} Cu(I)-binding site, without dissociation of bound Cu(I) into the solvent.

Sco^{Sl} has previously been shown to be essential for morphological development [26]. Therefore a role for ECuC in morphological development would be expected based on the *in vitro* data revealing ECuC as a Cu(I) donor for Sco^{Sl}. However, morphological development in the Δ*ecuc* mutant is similar to that of the WT (Figure 9A), whereas the CcO activity in the mutant is significantly reduced (45 % of WT activity, Figure 9B). This underscores that morphological development does not depend on the level of CcO activity [26] and furthermore demonstrates the involvement of ECuC together with Sco^{Sl} in CcO maturation. A model for extracytoplasmic Cu trafficking in *S. lividans* may include a direct functional link between ECuC and a putative Cu transporter encoded by *SLI4212*, adjacent to ECuC (*SLI4213*). It has been suggested that cuproproteins and chaperones may be co-factored following the re-routing of extracytoplasmic/periplasmic Cu via the cytosol and redelivered as Cu(I) by P_1-type ATPases [54]. As Cu(II)–ECuC could not be detected *in vitro*, we infer that efficient Cu(I) loading of ECuC at low [Cu] *in vivo* may depend on the SLI4212 transporter and an imbalance in (temporal) expression or localization of the two proteins may therefore hamper the efficiency of CcO maturation (Figure 9B).

We have previously demonstrated the requirement for Cu(II)–Sco^{Sl} and not Cu(I)–Sco^{Sl} to rescue CcO activity in the Δ*sco* mutant [26]. One could envisage that Sco^{Sl} to some extent could scavenge Cu(II) directly from extracytoplasmic pools at low [Cu] without the need for another chaperone, whereas complete and efficient loading requires ECuC as a Cu(I) donor and then the subsequent requirement of an oxidizing molecule or protein. This scenario fits with the observation that for morphological development to take place ECuC is not required, suggesting that delivery of Cu to another Sco^{Sl} target, which we predicted previously to be a cuproenzyme involved in the initiation of aerial hyphae [26], does not depend on ECuC as a Cu(I) donor. Thus in *S. lividans* extracytoplasmic Cu trafficking appears to be a branched pathway, where one branch requires both Sco^{Sl} and ECuC to participate in cofactoring the Cu_A domain of CcO, whereas the other branch, which awaits full characterization, uses only Sco^{Sl} to deliver Cu and initiate development.

AUTHOR CONTRIBUTION

Jonathan Worrall and Erik Vijgenboom conceived and designed the project. Katie Blundell, Michael Hough and Erik Vijgenboom carried out experimental work. All authors analysed and interpreted the data, and contributed to the writing of the paper.

ACKNOWLEDGEMENT

We thank the Diamond Light Source for access to beamlines I02, I03and I24 (East of England Macromolecular Crystallography BAG, MX7461).

FUNDING

K.L.I.M.B. is funded by a Ph.D. studentship from the University of Essex.

REFERENCES

1 Macomber, L. and Imlay, J. A. (2009) The iron-sulfur clusters of dehydratases are primary intracellular targets of copper toxicity. Proc. Natl. Acad. Sci. U.S.A. **106**, 8344 – 8349
2 Pufahl, R. A., Singer, C. P., Peariso, K. L., Lin, S. J., Schmidt, P. J., Fahrni, C. J., Culotta, V. C., Penner-Hahn, J. E. and O'Halloran, T. V. (1997) Metal ion chaperone function of the soluble Cu(I) receptor Atx1. Science **278**, 853–856
3 O'Halloran, T. V. and Culotta, V. C. (2000) Metallochaperones, an intracellular shuttle service for metal ions. J. Biol. Chem. **275**, 25057–25060
4 Robinson, N. J. and Winge, D. R. (2010) Copper metallochaperones. Annu. Rev. Biochem. **79**, 537–562
5 Arnesano, F., Banci, L., Bertini, I., Cantini, F., Ciofi-Baffoni, S., Huffman, D. L. and O'Halloran, T. V. (2001) Characterization of the binding interface between the copper chaperone Atx1 and the first cytosolic domain of Ccc2 ATPase. J. Biol. Chem. **276**, 41365–41376
6 Banci, L., Bertini, I., Cantini, F., Chasapis, C. T., Hadjiliadis, N. and Rosato, A. (2005) A NMR study of the interaction of a three-domain construct of ATP7A with copper(I) and copper(I)-HAH1: the interplay of domains. J. Biol. Chem. **280**, 38259–38263
7 Banci, L., Bertini, I., Cantini, F., Felli, I. C., Gonnelli, L., Hadjiliadis, N., Pierattelli, R., Rosato, A. and Voulgaris, P. (2006) The Atx1-Ccc2 complex is a metal-mediated protein-protein interaction. Nat. Chem. Biol. **2**, 367–368
8 Banci, L., Bertini, I., Ciofi-Baffoni, S., Kandias, N. G., Robinson, N. J., Spyroulias, G. A., Su, X. C., Tottey, S. and Vanarotti, M. (2006) The delivery of copper for thylakoid import observed by NMR. Proc. Natl. Acad. Sci. U.S.A. **103**, 8320–8325
9 Abriata, L. A., Banci, L., Bertini, I., Ciofi-Baffoni, S., Gkazonis, P., Spyroulias, G. A., Vila, A. J. and Wang, S. (2008) Mechanism of Cu(A) assembly. Nat. Chem. Biol. **4**, 599–601
10 Tsukihara, T., Aoyama, H., Yamashita, E., Tomizaki, T., Yamaguchi, H., Shinzawa-Itoh, K., Nakashima, R., Yaono, R. and Yoshikawa, S. (1996) The whole structure of the 13-subunit oxidized cytochrome c oxidase at 2.8 Å. Science **272**, 1136–1144
11 Horng, Y. C., Cobine, P. A., Maxfield, A. B., Carr, H. S. and Winge, D. R. (2004) Specific copper transfer from the Cox17 metallochaperone to both Sco1 and Cox11 in the assembly of yeast cytochrome c oxidase. J. Biol. Chem. **279**, 35334–35340
12 Tzagoloff, A., Capitanio, N., Nobrega, M. P. and Gatti, D. (1990) Cytochrome oxidase assembly in yeast requires the product of COX11, a homolog of the *P. denitrificans* protein encoded by ORF3. EMBO J. **9**, 2759–2764
13 Hiser, L., Di Valentin, M., Hamer, A. G. and Hosler, J. P. (2000) Cox11p is required for stable formation of the Cu(B) and magnesium centers of cytochrome c oxidase. J. Biol. Chem. **275**, 619 – 623
14 Glerum, D. M., Shtanko, A. and Tzagoloff, A. (1996) SCO1 and SCO2 act as high copy suppressors of a mitochondrial copper recruitment defect in *Saccharomyces cerevisiae*. J. Biol. Chem. **271**, 20531–20535
15 Rentzsch, A., Krummeck-Weiss, G., Hofer, A., Bartuschka, A., Ostermann, K. and Rodel, G. (1999) Mitochondrial copper metabolism in yeast: mutational analysis of Sco1p involved in the biogenesis of cytochrome c oxidase. Curr. Genet. **35**, 103–108
16 Nittis, T., George, G. N. and Winge, D. R. (2001) Yeast Sco1, a protein essential for cytochrome c oxidase function is a Cu(I)-binding protein. J. Biol. Chem. **276**, 42520–42526
17 Banci, L., Bertini, I., Cavallaro, G. and Ciofi-Baffoni, S. (2011) Seeking the determinants of the elusive functions of Sco proteins. FEBS J. **278**, 2244–2262
18 Banci, L., Bertini, I., Ciofi-Baffoni, S., Katsari, E., Katsaros, N., Kubicek, K. and Mangani, S. (2005) A copper(I) protein possibly involved in the assembly of CuA center of bacterial cytochrome c oxidase. Proc. Natl. Acad. Sci. U.S.A. **102**, 3994–3999
19 Serventi, F., Youard, Z. A., Murset, V., Huwiler, S., Buhler, D., Richter, M., Luchsinger, R., Fischer, H. M., Brogioli, R., Niederer, M. and Hennecke, H. (2012) Copper starvation-inducible protein for cytochrome oxidase biogenesis in *Bradyrhizobium japonicum*. J. Biol. Chem. **287**, 38812–38823
20 Thompson, A. K., Gray, J., Liu, A. and Hosler, J. P. (2012) The roles of *Rhodobacter sphaeroides* copper chaperones PCu(A)C and Sco (PrrC) in the assembly of the copper centers of the aa_3-type and the cbb_3-type cytochrome c oxidases. Biochim. Biophys. Acta **1817**, 955–964
21 Cruz-Morales, P., Vijgenboom, E., Iruegas-Bocardo, F., Girard, G., Yanez-Guerra, L. A., Ramos-Aboites, H. E., Pernodet, J. L., Anne, J., van Wezel, G. P. and Barona-Gomez, F. (2013) The genome sequence of S*treptomyces lividans* 66 reveals a novel tRNA-dependent peptide biosynthetic system within a metal-related genomic island. Genome Biol. Evol. **5**, 1165–1175
22 Kieser, T. and Hopwood, D. A. (1991) Genetic manipulation of *Streptomyces*: integrating vectors and gene replacement. Methods Enzymol. **204**, 430–458
23 Ueda, K., Tomaru, Y., Endoh, K. and Beppu, T. (1997) Stimulatory effect of copper on antibiotic production and morphological differentiation in *Streptomyces tanashiensis*. J. Antibiot. (Tokyo) **50**, 693–695
24 Keijser, B. J., van Wezel, G. P., Canters, G. W., Kieser, T. and Vijgenboom, E. (2000) The ram-dependence of *Streptomyces lividans* differentiation is bypassed by copper. J. Mol. Microbiol. Biotechnol. **2**, 565–574
25 Fujimoto, M., Yamada, A., Kurosawa, J., Kawata, A., Beppu, T., Takano, H. and Ueda, K. (2012) Pleiotropic role of the Sco1/SenC family copper chaperone in the physiology of *Streptomyces*. Microbiol. Biotechnol. **5**, 477–488
26 Blundell, K. L. I. M., Wilson, M. T., Svistunenko, D. A., Vijgenboom, E. and Worrall, J. A. R. (2013) Morphological development and cytochrome c oxidase activity in *Streptomyces lividans* are dependent on the action of a copper bound Sco protein. Open Biol. **3**, 120163
27 Worrall, J. A. R. and Vijgenboom, E. (2010) Copper mining in *Streptomyces*: enzymes, natural products and development. Nat. Prod. Rep. **27**, 742–756
28 Mattatall, N. R., Jazairi, J. and Hill, B. C. (2000) Characterization of YpmQ, an accessory protein required for the expression of cytochrome c oxidase in *Bacillus subtilis*. J. Biol. Chem. **275**, 28802–28809
29 Siluvai, G. S., Nakano, M., Mayfield, M. and Blackburn, N. J. (2011) The essential role of the Cu(II) state of Sco in the maturation of the Cu(A) center of cytochrome oxidase: evidence from H135Met and H135SeM variants of the *Bacillus subtilis* Sco. J. Biol. Inorg. Chem. **16**, 285–297
30 Blundell, K. L. I. M., Wilson, M. T., Vijgenboom, E. and Worrall, J. A. R. (2013) The role of the Cys-X-X-X-Cys motif on the kinetics of cupric ion loading to the *Streptomyces lividans* Sco protein. Dalton Trans. **42**, 10608–10616
31 Kieser, T. B., Bibb, M. J., Buttner, M. J., Chater, K. F. and Hopwood, D. A. (2000) Practical *Streptomyces* Genetics, John Innes Foundation, Norwich, U.K.
32 Green, G. N. and Gennis, R. B. (1983) Isolation and characterization of an *Escherichia coli* mutant lacking cytochrome *d* terminal oxidase. J. Bacteriol. **154**, 1269–1275
33 Mueller, J. P. and Taber, H. W. (1989) Isolation and sequence of ctaA, a gene required for cytochrome aa3 biosynthesis and sporulation in *Bacillus subtilis*. J. Bacteriol. **171**, 4967–4978
34 Gasteiger, E., Gattiker, A., Hoogland, C., Ivanyi, I., Appel, R. D. and Bairoch, A. (2003) ExPASy: the proteomics server for in-depth protein knowledge and analysis. Nucleic Acids Res. **31**, 3784–3788
35 Whitmore, L. and Wallace, B. A. (2004) DICHROWEB, an online server for protein secondary structure analyses from circular dichroism spectroscopic data. Nucleic Acids Res. **32**, W668–W673
36 Xiao, Z., Donnelly, P. S., Zimmermann, M. and Wedd, A. G. (2008) Transfer of copper between bis(thiosemicarbazone) ligands and intracellular copper-binding proteins. Insights into mechanisms of copper uptake and hypoxia selectivity. Inorg. Chem. **47**, 4338–4347
37 Xiao, Z., Loughlin, F., George, G. N., Howlett, G. J. and Wedd, A. G. (2004) C-terminal domain of the membrane copper transporter Ctr1 from *Saccharomyces cerevisiae* binds four Cu(I) ions as a cuprous-thiolate polynuclear cluster: sub-femtomolar Cu(I) affinity of three proteins involved in copper trafficking. J. Am. Chem. Soc. **126**, 3081–3090
38 Xiao, Z., Brose, J., Schimo, S., Ackland, S. M., La Fontaine, S. and Wedd, A. G. (2011) Unification of the copper(I) binding affinities of the metallo-chaperones Atx1, Atox1, and related proteins: detection probes and affinity standards. J. Biol. Chem. **286**, 11047–11055
39 Battye, T. G., Kontogiannis, L., Johnson, O., Powell, H. R. and Leslie, A. G. (2011) iMOSFLM: a new graphical interface for diffraction-image processing with MOSFLM. Acta Crystallogr. D Biol. Crystallogr. **67**, 271–281
40 Evans, P. (2006) Scaling and assessment of data quality. Acta Crystallogr. D Biol. Crystallogr. **62**, 72–82
41 Adams, P. D., Afonine, P. V., Bunkoczi, G., Chen, V. B., Davis, I. W., Echols, N., Headd, J. J., Hung, L. W., Kapral, G. J., Grosse-Kunstleve, R. W et al. (2010) PHENIX: a comprehensive Python-based system for macromolecular structure solution. Acta Crystallogr. D Biol. Crystallogr. **66**, 213–221
42 Cowtan, K. (2006) The Buccaneer software for automated model building. 1. Tracing protein chains. Acta Crystallogr. D Biol. Crystallogr. **62**, 1002–1011
43 Perrakis, A., Morris, R. and Lamzin, V. S. (1999) Automated protein model building combined with iterative structure refinement. Nat. Struct. Biol. **6**, 458–463
44 Murshudov, G. N., Vagin, A. A. and Dodson, E. J. (1997) Refinement of macromolecular structures by the maximum-likelihood method. Acta Crystallogr. D Biol. Crystallogr. **53**, 240–255
45 Emsley, P. and Cowtan, K. (2004) Coot: model-building tools for molecular graphics. Acta Crystallogr. D Biol. Crystallogr. **60**, 2126–2132
46 Davis, I. W., Leaver-Fay, A., Chen, V. B., Block, J. N., Kapral, G. J., Wang, X., Murray, L. W., Arendall, 3rd, W. B., Snoeyink, J., Richardson, J. S. and Richardson, D. C. (2007) MolProbity: all-atom contacts and structure validation for proteins and nucleic acids. Nucleic Acids Res. **35**, W375–W383
47 Long, F., Vagin, A. A., Young, P. and Murshudov, G. N. (2008) BALBES: a molecular-replacement pipeline. Acta Crystallogr. D Biol. Crystallogr. **64**, 125–132
48 Sreerama, N. and Woody, R. W. (2003) Structural composition of betal- and betall-proteins. Protein Sci. **12**, 384–388

49 Ledwidge, R., Hong, B., Dotsch, V. and Miller, S. M. (2010) NmerA of Tn501 mercuric ion reductase: structural modulation of the pKa values of the metal binding cysteine thiols. Biochemistry **49**, 8988–8998
50 Badarau, A. and Dennison, C. (2011) Copper trafficking mechanism of CXXC-containing domains: insight from the pH-dependence of their Cu(I) affinities. J. Am. Chem. Soc. **133**, 2983–2988
51 Banci, L., Bertini, I., Ciofi-Baffoni, S., Kozyreva, T., Zovo, K. and Palumaa, P. (2010) Affinity gradients drive copper to cellular destinations. Nature **465**, 645–648
52 Badarau, A. and Dennison, C. (2011) Thermodynamics of copper and zinc distribution in the cyanobacterium Synechocystis PCC 6803. Proc. Natl. Acad. Sci. U.S.A. **108**, 13007–13012
53 Rodriguez-Granillo, A., Crespo, A., Estrin, D. A. and Wittung-Stafshede, P. (2010) Copper-transfer mechanism from the human chaperone Atox1 to a metal-binding domain of Wilson disease protein. J. Phys. Chem. B. **114**, 3698–3706
54 Waldron, K. J., Firbank, S. J., Dainty, S. J., Perez-Rama, M., Tottey, S. and Robinson, N. J. (2010) Structure and metal loading of a soluble periplasm cuproprotein. J. Biol. Chem. **285**, 32504–32511

Received 2 January 2014/14 February 2014; accepted 19 February 2014
Published as BJ Immediate Publication 19 February 2014, doi:10.1042/BJ20140017

Biochem. J. (2014) **459**, 525–538 (Printed in Great Britain) doi:10.1042/BJ20140017

online data

SUPPLEMENTARY ONLINE DATA

Structural and mechanistic insights into an extracytoplasmic copper trafficking pathway in *Streptomyces lividans*

Katie L. I. M. BLUNDELL*, Michael A. HOUGH*, Erik VIJGENBOOM† and Jonathan A. R. WORRALL*[1]

*School of Biological Sciences, University of Essex, Wivenhoe Park, Colchester CO4 3SQ, U.K.

†Molecular Biotechnology, Institute of Biology, Sylvius Laboratory, Leiden University, PO Box 9505, 2300RA Leiden, The Netherlands

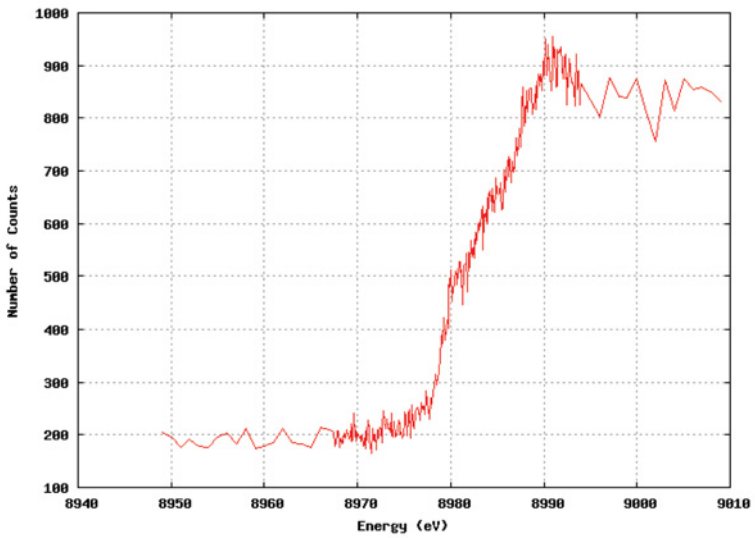

Figure S1 X-ray fluorescence scan at the Cu edge for a single crystal of *S. lividans* Cu(I)–ECuC

[1] To whom correspondence should be addressed (email jworrall@essex.ac.uk).

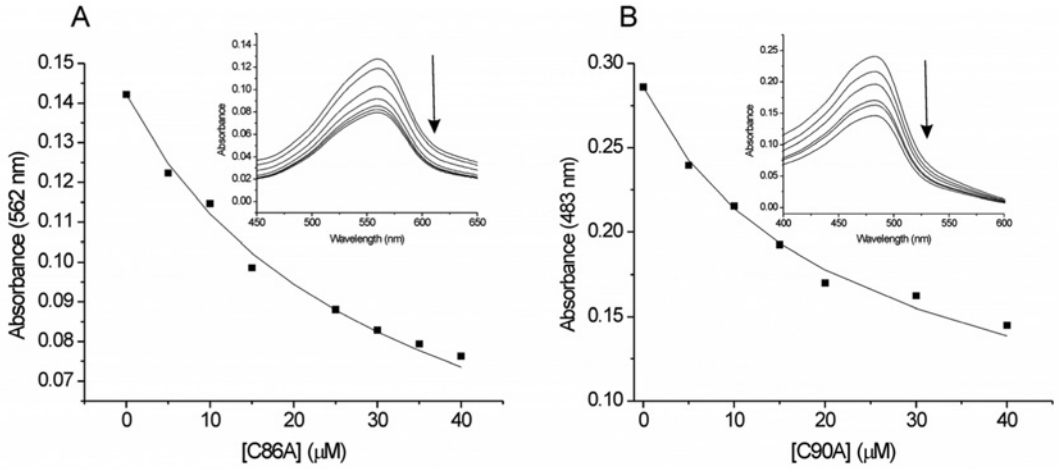

Figure S2 Determination of the $K_d(Cu^I)$ for the C86A and C90A mutants of Sco^{SI}

(**A**) The $K_d(Cu^I)$ for the C86A mutant was determined using $[Cu^I(BCA)_2]^{3-}$ as a competitive probe under Cu(I)-limiting conditions. Inset: the absorbance at 562 nm in the visible spectrum of $[Cu^I(BCA)_2]^{3-}$ decreases upon the addition of the C86A Sco^{SI} mutant with a plot of this absorbance change against [C86A] to determine the $K_d(Cu^I)$ using eqn (2) of the main text. The line through the data points represents a best fit to the data using a $K_d(Cu^I)$ of 7.3×10^{-14} M. Conditions used: 0–40 μM [C86A], 18 μM $[Cu^I]_{total}$ and 75 μM [BCA]. (**B**) The $K_d(Cu^I)$ for the C90A mutant was determined using $[Cu^I(BCS)_2]^{3-}$ as a competitive probe under Cu(I)-limiting conditions. Inset: the absorbance at 483 nm in the visible spectrum of $[Cu^I(BCS)_2]^{3-}$ decreases upon the addition of the C90A Sco^{SI} mutant with a plot of this absorbance change against [C90A] to determine the $K_d(Cu^I)$ using eqn (2) of the main text. The line through the data points represents a best fit to the data using a $K_d(Cu^I)$ of 2.9×10^{-16} M. Conditions used: 0–40 μM [C90A], 22 μM $[Cu^I]_{total}$ and 60 μM [BCS].

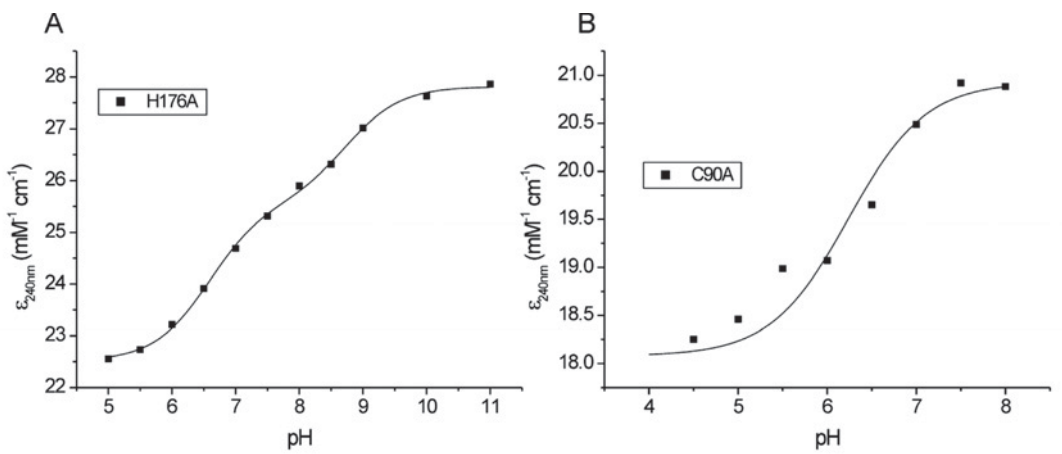

Figure S3 Determination of the pK_a values of the cysteine residues in the H176A (A) and C90A (B) mutants of Sco^{SI}

Changes in absorbance at 240 nm are plotted as a function of pH for the H176A (30 μM) and the C90A (30 μM) mutants of Sco^{SI}. For H176A the data points are fitted to two ionizations (eqn 4) and for the C90A mutant a single ionization process (eqn 3).

Received 2 January 2014/14 February 2014; accepted 19 February 2014
Published as BJ Immediate Publication 19 February 2014, doi:10.1042/BJ20140017